Opposing diet, microbiome and metabolite mechanisms regulate inflammatory bowel disease in a genetically susceptible host

Gabriel Vasconcelos Pereira[1,#], Marie Boudaud[2,#], Mathis Wolter[2,3], Celeste Alexander[1], Alessandro De Sciscio[2], Erica. T. Grant[2,3], Bruno Caetano Trindade[4], Nicholas A. Pudlo[1], Shaleni Singh[1], Austin Campbell[1], Mengrou Shan[4,7], Li Zhang[4,7], Qinnan Yang[1], Stéphanie Willieme[2], Kwi Kim[4], Trisha Denike-Duval[5], Jaime Fuentes[1], André Bleich[8], Thomas M. Schmidt[1,4,6], Lucy Kennedy[5], Costas A. Lyssiotis[4,7], Grace Y. Chen[4], Kathryn A. Eaton[1], Mahesh S. Desai[2,9,$,*], Eric C. Martens[1,$,§,*]

Affiliations:

[1]Department of Microbiology and Immunology, University of Michigan Medical School, Ann Arbor, Michigan, USA

[2]Department of Infection and Immunity, Luxembourg Institute of Health, 4354 Esch-sur-Alzette, Luxembourg

[3]Faculty of Science, Technology and Medicine, University of Luxembourg, 4365 Esch-sur-Alzette, Luxembourg

[4]Department of Internal Medicine, University of Michigan, Ann Arbor, Michigan, USA

[5]Unit for Laboratory Animal Medicine, University of Michigan, Ann Arbor, Michigan, USA

[6]Department of Ecology and Evolutionary Biology, University of Michigan, Ann Arbor, Michigan, USA

[7]Department of Molecular & Integrative Physiology, University of Michigan, Ann Arbor, Michigan, USA

[8]Institute for Laboratory Animal Science, Hanover Medical School, Hanover, Germany

[9]Odense Research Center for Anaphylaxis, Department of Dermatology and Allergy Center, Odense University Hospital, University of Southern Denmark, Odense, Denmark

[#]These authors contributed equally

*Correspondence to: emartens@umich.edu, mahesh.desai@lih.lu

[§]Lead author

[$]Senior author

Summary

Inflammatory bowel diseases (IBDs) are chronic conditions characterized by periods of spontaneous intestinal inflammation and are increasing in industrialized populations. Combined with host genetics, diet and gut bacteria are thought to contribute prominently to IBDs, but mechanisms are still emerging. In mice lacking the IBD-associated cytokine, Interleukin-10, we show that low dietary fiber promotes bacterial erosion of colonic mucus, leading to lethal colitis. A fiber-free exclusive enteral nutrition diet also induces mucus erosion but inhibits inflammation by simultaneously increasing an anti-inflammatory bacterial metabolite, isobutyrate. Diet-induced inflammation is driven by Th1 immune responses, which increase in the presence of mucin-degrading bacteria and are preceded by expansion of natural killer cells and altered immunoglobulin-A coating of some bacteria. Inflammation occurs first in intestinal regions with thinner mucus. Our work underscores the importance of focusing on microbial functions—not taxa—contributing to IBDs and some diet-mediated functions block those that promote disease.

Introduction

Inflammatory bowel diseases (IBDs) are characterized by periods of spontaneous inflammation in the gastrointestinal tract and occur in people with underlying genetic variations that cause inappropriate immune responses to intestinal antigens, especially ordinarily non-harmful symbiotic gut microbes[1]. Despite identification of hundreds of IBD-associated gene polymorphisms[2], precise mechanisms through which IBDs develop have not been determined. Even when predisposing genetics exist, IBDs do not always occur, suggesting that additional important triggers beyond host genetics and gut microbes are required[3].

The incidence of IBDs is increasing in some industrializing countries[4] and in immigrant populations that move to industrialized countries[5]. Dietary changes associated with industrialization (decreased fiber, increased processed foods, emulsifiers and sugars) are emerging as potential "triggers" that enhance susceptibility[6-9] and some underlying mechanisms are beginning to emerge[7,9]. The physiology of the microbes inhabiting the gut is continuously influenced by diet, especially fiber polysaccharides that elude digestion in the upper gastrointestinal tract and arrive in the colon providing nutrients for microbes[10-12]. Several studies using mice fed low fiber, high sugar or other "Westernized" diets have shown alterations in the microbiome that correlate with reduced integrity of the mucus barrier, including increased activity of mucin-degrading bacteria and reduced mucus thickness[9,13, ,14,15,16] and increased mucus penetrability[17].

We investigated the contributions of dietary fiber and mucin-degrading gut bacteria to the development of inflammation in mice lacking the IBD-associated cytokine Interleukin-10 (IL-10). In humans, loss of IL-10 or either of its receptor subunits results in early onset IBD in infants and children[18]. Conventional *Il10*$^{-/-}$ mice develop spontaneous inflammation that is variable between mouse colonies and worsened by the presence of pathobionts like *Enterococcus faecalis* or *Helicobacter* spp.[19], while deriving mice as germfree reduces or eliminates inflammation[20]. Thus, gut microbes are required for inflammation in *Il10*$^{-/-}$ mice, however, the mechanisms mediating disease progression in the presence of commensal bacteria lacking known pathogenic qualities remain unknown.

We found that a combination of IL-10 loss, gut microbiota containing mucin-degrading bacteria and a low-fiber diet, which promotes bacterial mucus erosion, are all required to elicit severe intestinal inflammation. We also observed that the clinically validated diet therapy

86 exclusive enteral nutrition (EEN) partially inhibits inflammation—despite lacking dietary fiber
87 and promoting mucus erosion—in part by promoting production of the bacterial metabolite
88 isobutyrate. Our work highlights the idea that microbial *functions* should be the focus of positive
89 and negative impacts in the development of IBDs. Some of these functions, like mucus
90 degradation, can be genetically complex and difficult to predict from taxonomic or metagenomic
91 data, necessitating the use of simplified systems in which individual functions contributing to
92 IBDs can be investigated at mechanistic levels prior to research in humans.

93

94 **Results**

95 ***A combination of host genetic susceptibility, low dietary fiber and intestinal bacteria***
96 ***exacerbate colitis in Il10$^{-/-}$ mice***

97 We previously determined that colonizing wild-type (WT) germfree mice with a
98 synthetic microbiota containing 14 species (SM14) of sequenced and metabolically characterized
99 human gut bacteria results in erosion of colonic mucus and increased *Citrobacter rodentium*
100 susceptibility in mice fed a fiber-free (FF) diet[13]. Fiber-deprived WT mice do not develop
101 spontaneous, histologically evident inflammation. Notably, mice colonized with the same SM14
102 and fed a fiber rich diet do not experience mucus erosion because metabolism of fiber by gut
103 bacteria decreases the abundance and activity of mucin-degrading species[13]. To determine if diet-
104 and microbiota-driven mucus erosion—and the correspondingly increased proximity of bacteria
105 to host tissue—promotes disease in mice that are genetically susceptible to IBD, we introduced
106 the SM14 into germfree *Il10$^{-/-}$* mice, choosing the C57BL/6J background that has been reported
107 to be *most* resistant to inflammation[19]. We colonized adult 7–10-week-old *Il10$^{-/-}$* mice fed a fiber-
108 rich (FR) diet, and switched a subset of the mice to the FF diet after 14 days of colonization,
109 monitoring body weight up to 60d (**Figure 1A**). Mice kept on the FR diet (n=14) maintained or
110 gained weight. In contrast, mice switched to the FF diet began losing weight 1–2 weeks after the
111 diet switch and experienced 89% lethality by 60d (n=27). Histology revealed neutrophil
112 infiltration, mucosal erosion, ulceration and edema in the ceca of FF-fed mice, but not those fed
113 FR (**Figure 1B**). These markers were lower in the ileum and colon (**Figure 1C**). Cecal
114 inflammation did not develop in SM14-colonized WT mice fed either diet (**Figure 1D**).
115 Measurements of neutrophil-derived Lipocalin-2 (LCN2) in the cecal lumen provided additional
116 data supporting severe inflammation in SM14-colonized *Il10$^{-/-}$* mice fed the FF diet (**Figure 1E**).

117 Experiments in which individual variables for diet (FR, FF), colonization (SM14, germfree) and
118 host genotype (WT, *Il10*$^{-/-}$) were individually manipulated support the conclusion that severe
119 inflammation and weight loss only develop in the context of three conditions: IL-10 deficiency,
120 SM14 colonization and FF diet (**Figures 1D,E, S1A–D)**.

121 Switching SM14-colonized *Il10*$^{-/-}$ mice to the FF diet rapidly induced a shift in bacterial
122 composition characterized by decreased fiber-degraders (*B. ovatus* and *E. rectale*) and increased
123 abundance of two of the four known mucin-degraders, *A. muciniphila* and *B. caccae* (**Figure**
124 **S1E**). A similar trend was observed in wild-type mice fed the FF diet, albeit with significantly
125 higher levels of *Escherichia coli* and *Bacteroides thetaiotaomicron* in *Il10*$^{-/-}$ mice (**Figure**
126 **S1F,G**). As expected, feeding the FF diet to *Il10*$^{-/-}$ mice resulted in reduced mucus thickness
127 (**Figure S1H–K**). We hypothesize that this erosion of protective mucus is critical for IBD
128 development by increasing bacterial contact with the epithelium and the dysregulated *Il10*$^{-/-}$
129 immune system. Supporting this idea, using bacteria-sized florescent beads in an *ex situ* mucus
130 penetrability assay[21] we determined that FF-fed *Il10*$^{-/-}$ mice have higher colonic mucus
131 penetrability and closer proximity of 1μm-sized beads to the host epithelium compared to their
132 FR-fed counterparts (**Figure 1F,G, S1L,M**). This increase in mucus penetrability was not as
133 pronounced in wild-type mice with SM14 (**Figures 1F,G)**.

134 Human disease associated with IL-10 dysfunction often presents as early or very early
135 onset IBD in children[18]. With this in mind, we modified our model to allow natural microbiota
136 transfer in the neonatal period, which also enables direct comparison to conventional specific
137 pathogen free (SPF) mice that are also colonized at birth. We colonized germfree *Il10*$^{-/-}$ adult
138 parents fed the FR diet, allowing their pups to be exposed to the maternal SM14 beginning at
139 birth. In pre-weaned pups, the SM14 took on a similar composition as adult FF fed mice (**Figure**
140 **S1N**) due to the lack of fiber and the fact that milk oligosaccharides share linkages with mucin
141 *O*-glycans[22]. Pups weaned to the FF diet began losing weight after ~39 days post weaning (dpw)
142 (**Figure 1H**) and experienced 100% mortality by 84 dpw (**Figure 1I**). In most experiments, we
143 harvested FR- and FF-fed groups at 79 dpw (100d old in University of Michigan facility), in
144 which case mortality among the FF mice was ~82% and all mice weaned to the FR diet survived
145 (**Figure S1O**). A separate group of FR-fed mice showed 100% survival when maintained for 129
146 dpw (150d total) as did wild-type mice fed either diet (**Figure 1I**). Weight loss in pups weaned to

147 the FF diet corresponded with increasing fecal LCN2 that initiated around the same time (~39
148 dpw) of declining weight (**Figure 1J**).

149 Interestingly, *Il10*$^{-/-}$ mice with a conventional SPF microbiota fed the FF diet did not lose
150 weight as severely as those colonized with SM14 (**Figure 1H**). Compared to SM14-colonized
151 mice fed the FF diet, SPF mice showed lower cecal LCN2 at 79 dpw (**Figure 1K**), and less
152 histological damage (**Figure S1P**), revealing that the more complex, murine microbiota does not
153 promote the same level of inflammation. However, SPF mice fed the FF diet *did* exhibit reduced
154 mucus thickness, albeit significantly less than SM14-colonized mice (**Figure 1L**), a point
155 addressed in more detail below.

156

157 ***Restoration of dietary fiber inhibits inflammation***

158 The FR and FF diets differ in several aspects of their composition beyond fiber (**Table**
159 **S1**). To more directly test fiber's contribution, we created versions of the FF diet in which 7.5%
160 of the glucose it contains was replaced with an equivalent amount of food grade, pure fiber from
161 oat, wheat or apple. High sugar has been shown to promote inflammation, including in *Il10*$^{-/-}$
162 mice, and this effect is reduced by replacing some sugar with starch that is digested by the host
163 in the small intestine[9]. As a control for reducing the sugar in our fiber-supplemented diets, we
164 created a diet containing 7.5% highly digestible starch, exchanging free glucose for a glucose
165 polymer available to the host via upper GI digestion. The presence of 7.5% fiber from either of
166 the three sources, but not starch, significantly reduced LCN2 (**Figure 1M**) as well as weight loss
167 and histopathology (**Figure S2A,B**). Even when all of the glucose (44%) was replaced with
168 digestible starch, adult mice colonized with the SM14 developed disease (**Figures 1M, S2A,B**).
169 This high starch diet more closely approximates a fiber poor human diet, which would be
170 expected to be rich in starchy foods, protein and fat, and still promotes inflammation, implying
171 that direct free sugar availability to the gut microbiota is not a major component of disease
172 development in this model. *Bacteroides ovatus*, a proficient degrader of the polysaccharides
173 expected to be present in the supplemental fibers[23], was one of the major responders, increasing
174 between 2–3 fold in relative abundance and this increase occurred at the expense of mucin-
175 degrading *Akkermansia muciniphila* and *Bacteroides caccae* (**Figure S2C–G**).

176 To determine if restoring dietary fiber to mice that had already been fed the disease-
177 promoting FF diet is capable of blocking inflammation, we returned colonized adult mice to the
178 FR diet at either 30d or 40d (16 or 26 days after being switched to FF). Both groups of mice that
179 were returned to FR exhibited no lethal weight loss (**Figure S2H**) and LCN2 levels and
180 histology at 60d were lower than mice maintained on the FF diet (**Figure 1N, O**). Interestingly,
181 temporal fecal LCN2 measurements showed that both groups experienced a peak of
182 inflammation after fiber had been restored, which then began declining, indicating that low fiber
183 induces disruption to the host–microbe homeostasis in which inflammation is a lagging effect
184 that can eventually be reset (**Figure 1N**).

185

186 ***The status of the mucus layer is a critical determinant in developing inflammation***

187 To more directly evaluate the disease-promoting role of mucin-degrading bacteria, we
188 colonized adult *Il10*$^{-/-}$ mice with a simpler synthetic microbiota containing only the 10 species
189 ("SM10") previously shown to be unable to grow on mucin oligosaccharides[13]. SM10-colonized
190 mice exhibited 100% survival on the FF diet until 60d post colonization (n=7), significantly
191 lower cecal LCN2 at 60d (**Figure 2A**) and reduced histological damage (**Figure 2B**).
192 Eliminating the mucin-degrading bacteria also decreased mucus thinning (**Figures 2C, S2I**).
193 Notably, SM10 colonized mice still exhibited some inflammation (**Figure 2B**). Consistent with
194 the idea that the absence of mucus-degrading bacteria slows, but does not fully block,
195 inflammatory activation of the dysregulated *Il10*$^{-/-}$ immune system, SM10-colonized mice that
196 were switched to the FF diet for 136d (150d total colonization) exhibited significantly better
197 survival (50%) compared to FF-fed SM14 mice (**Figure 2D**).

198 Adding back single mucin-degrading bacteria to the SM10 did not elicit the same level of
199 LCN2 observed with the full SM14 at 60d, indicating that multiple species may act
200 synergistically (**Figure 2A**). Despite a lack of weight loss (not shown) and lower LCN2 at 60d,
201 the presence of either *B. thetaiotaomicron* or *A. muciniphila* as the sole mucin-degrader did elicit
202 histological inflammation in the cecum at 60d that was statistically identical to the full SM14
203 (**Figure 2B**), indicating that weight loss and LCN2 phenotypes can in some cases be separate
204 from histological damage. A longer, 150d experiment in which mucin-degrading *B.*
205 *thetaiotaomicron* was added back to the SM10 revealed that it significantly accelerated lethal
206 weight loss (**Figure 2D**) and caused histological inflammation that was worse in the cecum

207 (**Figure 2E**). Thus, this commensal acts like a conditional pathogen in the compromised *Il10*$^{-/-}$
208 host. Interestingly, the elevated cecal histology in SM+*Bt* colonized mice also occurred without
209 elevated LCN2 (**Figure 2F**). Finally, consistent with the idea that low dietary fiber promotes the
210 general proliferation of mucin-degrading bacteria, mice colonized with SM10 plus a single
211 mucin degrader all exhibited expansion of that mucin-degrading bacterium (**Figure S2J–O**).
212 This contrasts with SM14-colonized mice, which only show expansion of *Akkermansia*
213 *muciniphila* and *B. caccae* in response to low fiber (**Figure S2J**), implying that some mucin
214 degraders out compete others.

215 The FR diet could suppress inflammation through mechanisms unlinked to its role in
216 blocking mucin-degrading bacteria. As a separate test of the protective role for mucus in the
217 context of the FR diet, we bred *Il10*$^{-/-}$*Muc2*$^{-/-}$ double knockout (DKO) germfree mice, colonized
218 them with the SM14 and fed either the FR or FF diets. These mice lost weight quickly and
219 needed to be sacrificed regardless of diet (**Figure 2H**) and both groups exhibited severe
220 inflammation (**Figure 2I-L**). Interestingly, with uniform elimination of MUC2, inflammation in
221 DKO mice developed throughout the lower intestine but was more severe in the colon than in the
222 cecum (**Figure 2K-M**). Since mucus is known to be thinner and patchier in the cecum compared
223 to colon[24], we interpret this to mean that inflammation occurs first in the cecum of SM14-
224 colonized *Il10*$^{-/-}$ mice (*i.e.*, with MUC2) because this is a site with high bacterial density and
225 patchier mucus causing it to be where the mucus barrier fails first (note that small intestine also
226 has thin mucus, but far fewer bacteria).

227 We further leveraged the DKO mice to measure how individual bacteria from different
228 phyla (*e.g.*, with different types of ligands for pattern recognition receptors) elicit inflammation
229 in the context of IL-10 deficiency and deficient mucus barrier. In support of the conclusion that a
230 variety of commensal bacteria can stimulate inflammation in this system, we observed that
231 monocolonization with two different Bacteroidetes (*B. thetaiotaomicron* and *B. uniformis*), *A.*
232 *muciniphila* (Verrucomicrobia) and *Eubacterium rectale* (Firmicutes) all resulted in strong
233 inflammation, albeit once more with variations in LCN2 (**Figure 2N-Q**).
234

235 ***Some human gut symbionts possess transferrable, pathogenic qualities between microbiomes***

236 Because SPF mice fed the FF diet did not develop inflammation as severe as SM14-
237 colonized mice (**Figure 1H,K**), we performed co-housing experiments in which pups born to

238 SPF- and SM14-colonized mothers were mixed at weaning and exposed to each other's
239 microbiomes. Co-housing SM14-colonized *Il10*$^{-/-}$ pups with SPF mice prevented the weight loss
240 phenotype observed in response to FF-feeding (**Figure 3A**). However, it did not reduce—and
241 even slightly increased—cecal inflammation as measured by LCN2 (**Figure 3B**) or histology
242 (**Figure 3C**), again indicating that weight loss and inflammation can be uncoupled in the
243 presence of different microbiota. Co-housed mice born to SPF mothers showed a more variable
244 response , with ~50% of these mice developing inflammation that was similar in severity to FF-
245 fed, SM14-colonized mice (**Figure 3B,C**). Time course analysis of fecal LCN2 revealed a larger
246 difference between co-housed and non-co-housed SPF mice, with co-housed SPF mice behaving
247 nearly identically to FF-fed SM14 (**Figure 3D,** solid purple).

248 Based on 16S rRNA gene sequencing, at least 6 members of the SM14 could be detected
249 in co-housed SPF mice, often transiently or near the end of the time course when inflammation
250 developed (**Figures 3E-G, S3A-I**). The most prominent of these invading bacteria was the
251 human commensal *E. coli* strain HS, which appeared in co-housed SPF mice around 28 dpw,
252 prior to the onset of inflammation, and gradually increased, eventually reaching levels >10% in
253 most mice (**Figure 3E,** solid purple). Two of the mucin-degrading SM14 bacteria (*A.*
254 *muciniphila* and *Ba. intestinihominis*) showed a similar trend, albeit reaching lower levels and
255 with variability among individual mice (**Figure 3F,G**). Two other bacteria (*C. aerofaciens* and
256 *B. uniformis*) showed transient increases around the time inflammation was increasing (~48 dpw)
257 and these organisms decreased thereafter (**Figure S3D,E**). A test of whether weekly gavages of
258 *E. coli* HS into SPF mice that were otherwise not exposed to SM14 bacteria failed to support the
259 hypothesis that this species is the sole cause of increased inflammation (**Figure S3J,K)**. Taken
260 together, these co-housing results demonstrate that some of the 14 human bacteria in our
261 synthetic microbiota are capable of transferring increased low fiber-induced inflammation to
262 mice colonized with a natively complex microbiota, extending the relevance of this diet-driven
263 model to more complex communities and implying that one or more of the SM14 bacteria is
264 endowed with conditional pathogenic qualities.

265

266 ***Certain gut bacteria and metabolites associated with exclusive enteral nutrition prevent***
267 ***inflammation despite mucus erosion***

268 A notable characteristic of the disease-promoting FF diet is that its macronutrient
269 composition resembles some exclusive enteral nutrition (EEN) diets used clinically to treat some
270 IBDs (**Table S1**). EEN diets often contain low or no fiber[25] and have proven to be effective at
271 inducing remission in humans, although precise mechanisms are still unknown[26]. To determine if
272 an EEN diet lacking fiber promotes inflammation in our gnotobiotic *Il10*$^{-/-}$ model, we weaned
273 SM14-colonized pups onto a commercial EEN diet, which is normally taken as a liquid but in
274 this case was freeze-dried, pelleted and sterilized. The average weight trajectories of 15 mice
275 supported the conclusion that the low fiber EEN diet promotes some weight loss, although not as
276 severe as the FF diet (**Figure 4A**). Cecal LCN2 measurements and histology revealed
277 substantial disease variation in individual animals, with some mice resembling healthy FR-fed
278 mice, some resembling diseased FF-fed mice and some intermediate (**Figure 4B,C**). Despite
279 experiencing less inflammation, the EEN mice still exhibited reduced mucus thickness, which we
280 expected given the lack of fiber in the formula used (**Figure 4D**). Measurements of short- and
281 branched-chain fatty acids (SCFAs, BCFAs) revealed that mice fed the EEN diet displayed
282 between 43.2-723.0-fold (mean 133.4) elevated amounts of a single BCFA, isobutyrate (**Figure**
283 **4E**). Suggesting that higher production, might help suppress inflammation.

284 Isobutyrate is an isomer of the well-studied, anti-inflammatory short-chain fatty acid
285 butyrate, which did not increase (**Figure 4E**), and isobutyrate is derived from L-valine
286 fermentation by certain gut bacteria[27]. Two other BCFAs (2-methyl butyrate and isovalerate) did
287 not increase despite the amino acids they are derived from (L-leucine and L-isoleucine) being
288 present at similar abundance[28] in the soy and milk protein used in the EEN formulation (**Figure**
289 **4E**). This suggests that the increase in isobutyrate is not attributable to increased bulk dietary
290 protein fermentation, which should increase all three BCFAs. Providing either isobutyrate or
291 butyrate (35 mM) in the drinking water of mice fed the disease-promoting FF diet decreased
292 weight loss (**Figure 4F**) as well as inflammation (**Figure 4G,H**), revealing that either of these
293 molecules can offset the diet- and microbiome-induced damage.

294 EEN feeding promoted significant changes in the SM14, most notably 211-278-fold
295 increases (mean 255.6) in *E. rectale* relative abundance (**Figure 4I,** compare columns with red
296 asterisks). While this Firmicute is known to produce butyrate, measurements of culture
297 supernatants from 13 of the SM species in medium supplemented with L-valine revealed that *E.*
298 *rectale* does *not* produce isobutyurate under the conditions tested. Rather, isobutyrate was

299 produced by all 4 of the *Bacteroides,* plus *M. formatexigens* (**Figure 4J**). Nevertheless, to
300 determine if the large increase in *E. rectale* abundance was functionally connected with
301 isobutyrate production, we bred neonatal mice born to parents harboring a version of the SM14
302 but lacking *E. rectale* ("SM13 minus *E. rectale*") and fed them the EEN diet. Consistent with a
303 causal role for *E. rectale* in isobutyrate production, mice lacking *E. rectale* failed to produce
304 isobutyrate (**Figure 4K**). These mice also exhibited 40% lethality at 79dpw (**Figure 4L**),
305 although there was not a significant increase in cecal LCN2 levels or histology relative to the
306 EEN/SM14 group (**Figure 4M,N**).
307

308 ***Mucin-degrading bacteria mediate fiber deprivation-induced immune responses in a time- and***
309 ***location-dependent manner***

310 Development of intestinal inflammation is a complex process involving innate and
311 adaptive immune responses and critical roles for Th1/Th17 cells have been described in the *Il10*$^{-}$
312 $^{/-}$ colitis model in conventional/SPF mice[19]. Nevertheless, how specific microbial triggers
313 influence the underlying immune pathways and how responses develop over time are less clear.
314 We repeated the same SM14 and SM10 (non-mucin-degrading community) colonization
315 experiments described above with a different C57BL/6J line of *Il10*$^{-/-}$ mice (mouse facility:
316 University of Luxembourg) and observed similar weight loss in both adult and post-weaning FF-
317 fed mice colonized with SM14, but not SM10 (**Figure 5A-C**). Given the temporal variation in
318 colitis phenotypes in FF-fed SM14- (faster colitis) and SM10-colonized (slower colitis) *Il10*$^{-/-}$
319 mice, our model provides opportunities to investigate the contributions of not only the microbial
320 triggers (*i.e*., with or without mucin degraders) but the regionality (cecum vs. colon) of
321 inflammatory pathways associated with increased microbial mucin foraging during fiber
322 deficiency.

323 In FF-fed SM14-colonized mice, increased LCN2 was detected in the cecum as early as
324 35 dpw compared to FR and this diet effect was not observed in mice colonized with SM10 or
325 left germfree (**Figure 5D**). SM14 mice weaned onto the FF diet also exhibited higher fecal
326 LCN2 (a proxy for colon) than SM10 mice at 79 dpw, supporting a pro-inflammatory role of
327 mucin-degrading bacteria during fiber deprivation (**Figure 5D**). An expansion of natural killer
328 (NK) cells was detected in the cecum of FF-fed mice as soon as 35 dpw and this expansion was
329 similar in SM10- and SM14-colonized mice (**Figure 5E**, left panel; see **Figure S4A** for flow
330 cytometry sorting scheme and **S4B-I** for germfree *Il10*$^{-/-}$ and SM14-colonized WT controls for

331 flow cytometry experiments). In contrast to the pattern observed in cecum, NK cells expanded in
332 the colons of both FR and FF-fed SM14-colonized mice as soon as 35 dpw, but not in the colons
333 of SM10-colonized mice (**Figure 5E**, right panel). This further suggests that mucin-degrading
334 bacteria are more important to elicit responses in the colon where mucus is thicker and
335 degradation is required to increase contact. We also observed region-specific host responses that
336 are driven by diet x host genotype interactions, since FF-fed GF *Il10*$^{-/-}$ mice, but not SM14 or
337 SM10 colonized WT mice, showed increased NK cells in the cecum, but not in the colon, at 79
338 dpw compared to FR-fed controls (**Figure S4B**).

339 While NK cells were more abundant at 35 days and later decreased, T cell recruitment
340 increased over time, generally reaching highest levels at 79 dpw, in both the cecum and colon of
341 SM10- and SM14-colonized *Il10*$^{-/-}$ mice (**Figures S5A, S4C**). In the ceca of both SM10- and
342 SM14-colonized *Il10*$^{-/-}$ mice, the FF diet increased CD4^{+} and CD8^{+} T cell populations by 35
343 dpw, with CD4^{+} T cells increasing further by 79 dpw independently of the diet (**Figure 5F,G**).
344 However, CD4^{+} T cells also accumulated over time in the ceca of FF-fed GF *Il10*$^{-/-}$ mice (**Figure**
345 **S4D**), while CD8^{+} T cells were induced by FF-feeding in the ceca of GF *Il10*$^{-/-}$ mice, as well as in
346 the ceca and colons of SM14-colonized WT mice (**Figures S4E**). These results suggest that fiber
347 deprivation induces the recruitment of T cell populations through multiple paths and not all of
348 these are regulated by mucin-degrading bacteria, the microbiota and IL-10 deficiency.

349 Consistent with previous descriptions of *Il10*$^{-/-}$ colitis in conventional mice[19] both SM10-
350 and SM14-colonized mice generally exhibited infiltration of Th1 and Th17 cells over time
351 (**Figure 5H,I**) with fewer changes in Th2 cells (**Figure S5B**). Especially for Th17 cells, this
352 infiltration was higher in FF-fed mice in both the cecum and the colon (**Figure 5I**). While Th17
353 cells reached nearly equivalent levels at 79 dpw in SM10 and SM14-colonized ceca, overall
354 levels were lower in the SM10-colonized colons compared to SM14 (**Figure 5I**). Furthermore,
355 the FF diet increased Th1 levels in the SM14-colonized colons, but not in the SM10-colonized
356 ones (**Figure 5H**). Consistent with the readouts mentioned above, this observation supports the
357 idea that the role of mucin-degrading bacteria is more important in the colon where erosion of
358 mucus facilitates the induction of the anti-microbial Th1 responses.

359 Cytokine measurements in cecal tissues revealed expected increases in IBD-associated
360 markers IL-1β, IL-6, IL-17, IL-22, TNF-α and IFN-γ in fiber-deprived *Il10*$^{-/-}$ mice that were
361 colonized with SM14 as adults (**Figure 6A-F**).To provide functional support to the immune cell
362 profiles, we compared levels of Th1- and Th17-type cytokine transcripts in ceca and mesenteric

363 lymph nodes at 35 and 79 dpw in mice colonized at birth. In SM14-colonized *Il10*$^{-/-}$ mice, the FF
364 diet led to increased expression of Th1 (IFN-γ, IL-6, TNF-α, IL-12) and Th17 cytokines (IL-17F,
365 IL-22, IL-23 and TGF-β), as well as the mucin-inducing cytokine IL-13 (**Figures 6G-U**).
366 Interestingly, in the ceca of SM14-colonized mice, both Th1 and Th17 cytokines were induced at
367 35 dpw, while only Th1 cytokines were maintained at 79 dpw (**Figure 6G-N**). These cytokine
368 responses tended to develop more slowly in SM10-colonized ceca compared to those with SM14
369 and, both Th1 and Th17 cytokines were increased by 79 dpw in FF-fed SM10-colonized mice
370 (**Figure 6G-N**). In the colon-draining mesenteric lymph nodes (MLNs) where naïve T cells are
371 activated and polarized, the Th17-related cytokines, IL-17F and IL-22, were increased by FF-
372 feeding compared to FR in both SM10- and SM14-colonized mice (**Figure 6S-T**), while the
373 Th1-polarizing cytokines IFN-γ, IL-6 and IL-12 were only increased in SM14-colonized mice,
374 consistent with a dependence on mucin-degrading bacteria to develop Th1 responses (**Figures**
375 **6P-R**).
376 Despite the IL-10 deficiency, Foxp3^{+} regulatory T cell (Treg) recruitment was also higher
377 during FF feeding of SM14 *Il10*$^{-/-}$ mice (**Figures S5C-F**). This expansion being independent of
378 IL-10 suggests a mechanism driven by other regulatory mediators such as TGF-β, whose
379 transcript levels increased in SM14-colonized cecal tissues as soon as 35 dpw (**Figure 6N**).
380 Regulatory T cells expressing Tbet or RORγt have been proposed as counter-regulators of
381 inflammatory Th1 and Th17 cells, respectively[29,30]. Consistent with this, the abundance of Tbet^{+}
382 Treg cells follow the same trends as inflammatory Th1 cells with higher levels in FF-fed, SM14-
383 colonized mice (**Figures S5D**). By contrast, the highly suppressive RORγt^{+} Treg population was
384 reduced at 35 dpw in the colon and at 79 dpw in the cecum of FF-fed, SM14-colonized *Il10*$^{-/-}$
385 mice (**Figure S5E**), thus favoring inflammatory responses. In addition, Gata3^{+} Tregs were
386 increased in FF-fed colonized colons (**Figure S5F**). While their role in the specific regulation of
387 type 2 inflammatory cells is still unclear, they may constitute a reservoir of Tregs required for
388 tissue repair by 79 dpw in colonized colons[31,32]. Finally, despite the general expansion of Treg,
389 early (35 dpw) loss of the highly suppressive RORγt^{+} subset and the IL-10 deficiency are likely
390 to allow the Th1/Th17 responses to flourish in FF-fed, SM14 mice. Together, these results reveal
391 strong Th1/Th17 immune pathways induced by fiber deprivation, differentially regulated by
392 microbial community members and host genetics, in a time- and intestinal site-specific manner.
393
394

395 ***Alterations to IgA–microbiota interactions precede inflammation***

396 IgA production is a common anti-microbial response in the gut and is usually upregulated
397 during colitis in humans and mouse models[33]. Mirroring the LCN2 trend observed for early
398 inflammation (**Figure 6A**), soluble IgA titers were increased in the cecum at 35 dpw and the
399 feces at 79 dpw, in FF-fed SM14-colonized *Il10*$^{-/-}$ mice compared to FR, but not in SM10-
400 colonized mice (**Figure 7A**). However, prolonged FF-feeding (79 dpw) resulted in depletion of
401 plasma and IgA-producing cells in both the cecum and colon and this loss was also observed in
402 FF-fed WT mice that were colonized with SM14 (**Figure S6A, B**), suggesting a diet-driven
403 effect on IgA-producing cells rather than an effect of IL-10 loss. This is surprising considering
404 the increased levels of secreted IgA (**Figure 7A**), but consistent with a published report showing
405 reduced titers of serum IgA and fewer IgA^{+} B cells in the small intestine of wild-type mice fed a
406 zero-fiber diet compared to high-fiber[34]. In parallel with reduced IgA-producing cells after FF-
407 feeding, the proportion of IgG-producing B cells was increased at 35 and 79 dpw in both the
408 cecum and colon of SM14-colonized *Il10*$^{-/-}$ mice (**Figure S6C,D**). Consistent with the high
409 production of Th1 cytokines in the presence of mucin-degrading bacteria, FF-feeding increased
410 the proportion of IgG-producing cells only in SM14- but not in SM10-colonized colons (**Figure**
411 **S6D**)[35].

412 Since coating with immunoglobulin A (IgA) has been proposed to identify bacteria that
413 are potentially more colitogenic[36], we next focused on how the inflammation-promoting FF diet
414 alters bacterial IgA coating in *Il10*$^{-/-}$ mice. Consistent with previous studies[33], the amount of total
415 IgA-coated bacteria was higher in FF-fed mice than in FR-fed mice at 79 dpw (**Figure 7B**).
416 Along with increased luminal IgA (**Figure 7A**), this FF diet-induced increase in total IgA-
417 coating was not observed in SM10-colonized mice but was observed in SPF *Il10*$^{-/-}$ mice and
418 SM14-colonized WT mice, supporting a mechanism driven by mucin-degrading bacteria
419 (**Figures 7C, S7A**). Intriguingly, analysis of IgA-coated bacteria revealed the presence of 2
420 differentially coated populations in FR-fed mice: a large population with low-coating and a
421 smaller population with high coating, and both populations responded differently to FF-feeding
422 (**Figure 7D**). The proportion of low-coated bacteria increased in FF-fed mice, while the highly-
423 coated bacteria were almost completely lost in FF-fed mice, as early as 21 days of feeding
424 (**Figure 7D-F, S7B**). Additionally, highly-coated bacteria were diminished in SM10-colonized
425 mice as in SM14-colonized mice as soon as 21 dpw and low-coated bacteria only slightly
426 increased by 79 dpw (**Figure 7E,F, S7C**). Together these results suggest two levels of regulation

427 of IgA coating by the FF diet: a rapid loss of the high coating that occurs in the absence of
428 mucin-degrading bacteria, and a later increase of low and total coating that is partially dependent
429 on the mucin-degrading bacteria and likely linked to the increased secretion of IgA.
430 Interestingly, the EEN diet that dampened colitis but not mucus thinning in SM14-colonized
431 *Il10*$^{-/-}$ mice, increased the proportion of IgA-coated bacteria as soon as 21dpw and conserved the
432 high-coated population compared to mice fed FF (**Figure S7D**), suggesting additional immune-
433 regulatory properties of EEN diet components.

434 Given the altered pattern of overall IgA coating, we examined IgA coating of individual
435 SM14 bacteria. Consistent with the early loss of highly coated bacteria, changes in IgA-coating
436 of SM14 members also appeared as soon as 21 days of FF-feeding (**Figures 7G, S7E**). Among
437 the SM14 members, *A. muciniphila*, *D. piger*, *E. coli* and *C. aerofaciens* showed reduced IgA
438 coating index (ICI) values at one or both timepoints in FF-fed *Il10*$^{-/-}$ mice (**Figures 7G**). In WT
439 mice, this FF diet-induced reduction in IgA coating was less severe for *A. muciniphila*, but more
440 pronounced for *D. piger* and *C. aerofaciens*, revealing that IL-10 deficiency affects IgA-coating
441 of commensals in a species-dependent manner. In contrast, *E. rectale* showed a low ICI in FR-
442 fed mice and this increased with FF-feeding (**Figure 7G**), a condition in which it is present at
443 very low levels. The causes and effects of variations in IgA coating are still being determined.
444 However, our results demonstrate that different combinations of microbial colonization, diet and
445 host immune status can alter both the amount of intestinal IgA and the bacteria it targets. Along
446 with the data shown above, our results suggest the possibility that fiber deprivation initiates early
447 disruptions in IgA–microbiota interactions along with a loss of IgA-producing plasma cells.
448 Additional experiments to sort out the respective contributions of altered IgA coating vis-à-vis
449 alterations in microbiota physiology are made possible by these observations in a tractable
450 gnotobiotic system.

451

452 **Discussion**

453 The pathophysiology of IBDs is complex and variable, in part because of the large
454 number of different genetic contributions that combine with environmental, microbial and
455 dietary triggers known or hypothesized to influence its development. The diet-driven
456 inflammation model investigated here provides both a case study, in which contributing factors
457 to *Il10*$^{-/-}$-associated inflammation can be explored at mechanistic levels, as well as a more

458 general experimental paradigm in which host genetic, microbiota and dietary variables can be
459 manipulated to examine their effects on disease development. As examples of spontaneous,
460 genetically driven intestinal inflammation continue to be identified[37-39], the ability to work with
461 these murine models in germfree/gnotobiotic conditions and with defined diets holds the
462 potential to uncover foundational principles about these complex diseases.

463 An important conceptual idea that is supported by our findings is that opposing bacterial
464 functions influence disease outcomes. Low fiber induced mucus erosion is deleterious, but
465 mostly in the context of some members of the human SM14 community that appear to have
466 pathogenic qualities that can transfer their pro-inflammatory effect to SPF mice. During EEN
467 feeding, mucus erosion still occurs, but is offset to some degree by production of isobutyrate.
468 These opposing functions do not need to be mechanistically connected; rather, they may work
469 independently as long as the protective function (isobutyrate) is capable of reducing
470 inflammation that results from mucus thinning. Isobutyrate production is both influenced by diet
471 and contingent upon *E. rectale*. Thus, these data present actionable hypotheses for future work in
472 humans to determine if patients that respond positively to EEN also show increased isobutyrate
473 and if EEN responses can be stratified based on presence of *E. rectale*. Deconstruction of the
474 EEN formula to identify ingredients that promote *E. rectale*-dependent isobutyrate production, as
475 well as identifying the bacteria that produce isobutyrate *in vivo*, may also lead to optimization of
476 EEN formulations. These studies are ideally suited to be first conducted in a simplified pre-
477 clinical model that allows focus on individual contributions prior to extending to more complex
478 human studies.

479 The link between low dietary fiber and compromised thickness and/or permeability of the
480 mucus layer has been emerging through several studies[13,14,17,15,16]. Here, we make direct
481 functional connections between the dietary fiber-gut microbiome-mucus layer axis in the context
482 of IBD development in a genetically susceptible host in a way that depends on the specific
483 bacteria present (SM14 vs. SPF). Many questions remain regarding the development of the
484 multifactorial diseases called IBDs. While host genetics are a mostly permanent trait that is
485 difficult to repair, an exception being stem cell transplant in children lacking IL-10 signaling[40],
486 the microbiome and especially diet are factors that could be manipulated to delay or reverse
487 disease. Ever since the discovery that rearing *Il10*$^{-/-}$ mice under germfree conditions abrogates
488 inflammation[20], there has been substantial interest in finding specific bacteria that elicit

489 inflammation when added back to these animals. This search has yielded insight into the
490 contributions of bacteria with known pathogenic qualities, such as *Helicobacter* spp.,
491 *Enterococcus faecalis* and adherent invasive *E. coli*[19]. However, roles for specific commensal
492 bacteria have also been established using gnotobiotic mice[41], albeit without a clear understanding
493 of the mechanism(s) involved. Based on data presented here, we propose that it is appropriate to
494 focus more on the influence of positive and negative bacterial functions than on the role of
495 specific taxa. The rationale for this is that metabolic pathways like mucin degradation can be
496 present in diverse bacteria and some of these organisms may fulfill similar roles in eroding
497 mucus, while some may not. In contrast, strains of the same species can vary in key metabolic
498 capabilities, including mucus degradation, which is known to vary substantially among strains of
499 *Bacteroides*[42]. If one considers the effects of the microbiome on IBD development to be a
500 cumulative series of positive and negative stimuli caused by the particular behaviors and
501 metabolites exhibited by the microbes present, it should be possible to optimize beneficial
502 processes (*e.g.*, butyrate, isobutyrate) while reducing detrimental events like mucus erosion.
503 While some of these levers can be manipulated through diet, a promising path for intervention
504 may eventually include adding or replacing specific bacteria within a person's individual
505 microbiota with more optimal strains or perhaps even those that are engineered to increase
506 beneficial metabolites.

507

508 **Acknowledgements**

509 We thank the University of Michigan Germfree and Microbiome Cores for technical
510 assistance, Leonard Augenlicht for Muc2$^{-/-}$ mice and Bill Krueger (J. Rettenmaier) for fiber
511 samples. We are grateful for support from the Kenneth Rainin Foundation (Innovator Award,
512 ECM) and the US NIH (R01s DK118024, DK125445 to ECM; P01 HL149633 funding to CAL,
513 TMS and ECM). We thank the Luxembourg National Research Fund (FNR) for CORE grants
514 (C15/BM/10318186, C18/BM/12585940) and BRIDGES grant (22/17426243) to MSD and
515 MEDICE Arzneimittel Pütter GmbH & Co. KG, Germany and Theralution GmbH, Germany for
516 funding through the public–private partnership FNR BRIDGES grant to MSD (22/17426243).
517 MB was supported by a European Commission Horizon 2020 Marie Skłodowska-Curie Actions
518 individual fellowship (897408). MW was supported by a Fulbright grant for Visiting Scholars
519 from the Commission for Educational Exchange between the USA, Belgium and Luxembourg.

ETG was supported by FNR PRIDE (17/11823097). CA was supported by the University of Michigan Postdoctoral Translational Scholars Program.

Competing interest statement

ECM works as a consultant and an advisory board member at January, Inc, United States. MSD works as a consultant and an advisory board member at Theralution GmbH, Germany.

Figure Legends

Figure 1. Low fiber driven inflammation in *Il10*$^{-/-}$ mice. A. Weights of adult *Il10*$^{-/-}$ mice colonized with the SM14 and maintained on a fiber rich (FR) diet or switched to a fiber free (FF) diet at 14d. Curves represent polynomial (quadratic) equations fit to all of the weights gathered at various days. Weights were measured more frequently after 40d due to declining health in the FF group. Animals that were euthanized were excluded from the curve at later points. Two FF-fed animals from an early experiment were found dead and were not included in subsequent analyses. Right axis shows survival over time. **B.** Representative cecal histology of FF (left) and FR (right) fed SM14-colonized *Il10*$^{-/-}$ mice with higher magnification insets in the middle. Block arrows points to a large ulcer, line arrow to an area of edema. **C.** Quantitative, blinded histological scoring of ileal, cecal, and colonic tissue from colonized *Il10*$^{-/-}$ mice fed the FF diet (n=15–20, one-way ANOVA and post hoc test with Holm-Šídák's multiple comparison test) **D.** Histological scoring of cecal tissue taken from colonized *Il10*$^{-/-}$ mice fed the FR and FF diets, along with additional treatments to manipulate diet, colonization and host genotype variables (n=5–20). **E.** Cecal Lipocalin-2 (LCN2) measurements in the same treatments shown in D (n=5–23). **F.** Mucus penetrability by 1 um-sized beads in the distal colon of *Il10*$^{-/-}$ and WT mice fed the FR and FF diets. **G.** Distance of 1 um-sized beads from the epithelium in the same mice in F. **H.** Weights of *Il10*$^{-/-}$ mice born to either SM14 or SPF parents and weaned to FR or FF. By 79d post weaning, only the SM14/FF group (red) displays weight loss. Curves are fit to weight data as in A. **I.** Survival curves for 4 separate groups of WT C57bl/6 or *Il10*$^{-/-}$ mice colonized by parental transfer of SM14 bacteria at birth. **J.** Fecal LCN2 measurements over time in SM14 colonized *Il10*$^{-/-}$ pups weaned to FR and FF. **K.** Endpoint cecal LCN2 in SM14 and SPF colonized mice (n=4–7). **L.** Mucus thickness measurements in SM14 and SPF colonized mice. Sample size indicated below each treatment group (n=4–5). **M.** Cecal LCN2 in mice fed versions

552 of the FF diet with glucose replaced by dietary fiber from apple, wheat, oat or soluble starch.
553 Concentrations of each supplement are noted below the ingredient (n=5–23). **N.** Fecal LCN2
554 measurements over time in SM14 colonized adult mice shifted to FF at 14d post colonization and
555 then shifted back to FR at either 30d or 40d. For each time point/treatment the mean is shown
556 along with individual points and error bars represent S.E.M. **O.** Endpoint histology of the cecal
557 tissue from mice shown in N. compared to mice maintained on FR or FF (n=5–20). Experiments
558 in panels F. and G. were done at the University of Luxembourg; all others were done at the
559 University of Michigan. In panels C, D, E, J, K, L, M, bold horizontal bar represents the mean
560 and lighter error bars the S.E.M. *P* values: * $\leq$ 0.05; ** $\leq$ 0.01; ** $\leq$ 0.001; *** $\leq$ 0.001; **** $\leq$
561 0.0001; ns = not significant. In panels D, E, K, L, M, N, O, two-way ANOVA and post hoc test
562 with Original FDR method of Benjamini and Hochberg was used for statistics.
563
564 **Figure 2. Mucus integrity is central to diet-induced inflammation. A.** Cecal LCN2
565 measurements at 60d after colonization in *Il10*$^{-/-}$ mice with full or reduced complexity synthetic
566 microbiota as indicated in the "Colonized" line below each graph: Full SM14, just the SM10
567 species that do not degrade mucin *O*-glycans, or SM10 plus individual mucin degraders, *B.*
568 *thetaiotaomicron* (*Bt*), *B. caccae* (*Bc*), *B. intestinhominis* (*Bi*) or *A. muciniphila* (*Am*) (n=7–23).
569 **B.** Cecal histology scores of the same treatment group shown in A (n=5–20). **C.** Mucus thickness
570 in SM10 colonized mice fed the FF diet (gray) compared to SM14 colonized mice fed either diet
571 (n=5). **D.** Survival curves of *Il10*$^{-/-}$ adult mice colonized with SM14, SM10 and SM10+*Bt* to
572 150d. **E.** Regional histology of gastrointestinal tissues from SM10+*Bt*. **F.** Cecal LCN2 from
573 SM14 and SM10+*Bt* colonized mice. **G.** Representative histology from SM10, SM10+*Bt* and
574 SM10+*Am* at 60d. **H.** Survival curves of *Il10*$^{-/-}$ and DKO adult mice colonized with the SM14.
575 **I.-L.** Individual endpoint weight loss (I.), Cecal LCN2 (J.), colon histology (K.) and cecal
576 histology (L.) for SM14-colonized *Il10*$^{-/-}$*Muc2*$^{-/-}$ double knockout (DKO) mice fed the FR or FF
577 diets (n=5-23). **M.** Colon histology in *Il10*$^{-/-}$ (right) and DKO (left) mice showing worse disease
578 in DKO mice. **N.** Survival curves of mono-colonized DKO adult mice. **O-Q.** Cecal LCN2 (O.),
579 colon histology (P.) and cecum histology (Q.) of mice shown in N. In panels A, B, I-K, O bold
580 horizontal bar represents the mean and lighter error bars the S.E.M. In panels A-C, I-K, O two-
581 way ANOVA and post hoc test with Original FDR method of Benjamini and Hochberg was used
582 for statistics.
583

584 **Figure 3. Co-housing SPF- and SM14-colonized mice after weaning worsens disease. A.**
585 Weights of SPF or SM14-colonized mice co-housed at weaning (21d) with pups harboring the
586 opposite colonization. **B.** Cecal LCN2 levels in co-housed or non-co-housed SPF and SM14
587 mice (co-housing status is indicated at the bottom of this and other panels; n=5-11, one-tailed
588 Student's t-test and Wilcoxon test). **C.** Cecal histology of the same treatments shown in B (n=5-
589 11, one-tailed Student's t-test and Wilcoxon test). **D.** Cecal LCN2 over time in co-housed and
590 non-co-housed SPF and SM14 mice. **E–G.** Relative abundances of select SM14 species invading
591 SPF co-housed mice, *E. coli*, *A. muciniphila*, *Ba. intestinihominis*, respectively. Data are
592 represented as mean ± SEM. *p < 0.05; **p < 0.01; ***p < 0.001; ****p < 0.0001.
593
594 **Figure 4. Fiber free EEN diet improves inflammation in part through isobutyrate**
595 **production. A.** Weights of mice weaned onto FR, FF, and EEN diets. **B.** Cecal LCN2 levels in
596 mice weaned onto FF, FR, and EEN diets (n=7-15). **C.** Cecal histology scores of the mice shown
597 in B. (n=7-15). **D.** Mucus thickness measurements in mice shown in B.-C. (n=5). **E.** Short- and
598 branched-chain fatty acid measurements in mice fed FF, FR, or EEN diets (n=5-15). **F.** Weights
599 of mice fed the FF diet and water supplemented with either 35mM isobutyrate (orange) or
600 butyrate (purple) (n=6-15). **G.** Cecal LCN2 levels in the mice from panel F. **H.** Cecal histology
601 scores of the mice shown in F. (n=6-15). **I.** SM14 community composition in mice fed the FR,
602 FF and EEN diets. Red asterisks denote FF and EEN diet comparison. **J.** Short- and branched-
603 chain fatty acid measurements in culture supernatants of indvidual SM14 bacteria. **K.** Short and
604 branched chain fatty acid measurements in EEN fed mice colonized with either the full SM14 or
605 an SM13 lacking *E. rectale* (n=6-15, one-tailed Student's t-test and Wilcoxon test). **L.** Survival
606 of SM14 and SM13 (minus *E. rectale*) colonized mice on the FF and EEN diets. **M.** Cecal LCN2
607 measurements of the mice shown in L. (n=6-15, one-tailed Student's t-test and Wilcoxon test). **N.**
608 Cecal histology scores of the mice shown in L. (n=10,15). Data are represented as mean ± SEM.
609 *p < 0.05; **p < 0.01; ***p < 0.001; ****p < 0.0001. In panels B, C, D, E, G, H, two-way
610 ANOVA and post hoc test with Original FDR method of Benjamini and Hochberg was used for
611 statistics.
612
613 **Figure 5. Mucin-degrading bacteria mediate low fiber-induced immune responses in a**
614 **time- and location-dependent manner. A.–B.** Weights of SM14-colonized adult *Il10*$^{-/-}$ mice
615 (**A.,** n=6–10) and *Il10*$^{-/-}$ pups born to SM14- or SM10-colonized dams (**B.,** n=8–12), reproduced

616 in the University of Luxembourg mouse facility. **C.** Endpoint weights of individual animals
617 shown in B. (n=8–12). **D.** LCN2 levels in the cecal contents and feces of GF and colonized *Il10*$^{-/-}$
618 mice (n=4–7). Numbers on the X axis indicate the number of samples in which LCN2 was not
619 detected. **E.** Proportion of NK cells among CD3^{-}CD45^{+} cells in the cecum and colon lamina
620 propria of SM10- and SM14-colonized *Il10*$^{-/-}$ mice (n=4–11). **F–I.** Proportion of CD3^{+}CD4^{+} (**F.**),
621 CD3^{+}CD8^{+} (**G.**), Th1 (**H.**) and Th17 (**I.**) cells among CD45^{+} cells in the cecum and colon of
622 SM10- and SM14-colonized *Il10*$^{-/-}$ mice (n=4–11). Helper T (Th) cell subsets are defined as
623 CD3^{+} CD4^{+} Foxp3^{-}. Data are represented as mean ± SD. *p < 0.05; **p < 0.01; ***p < 0.001;
624 ****p < 0.0001. In panels C-I, two-way ANOVA and post hoc test with Original FDR method of
625 Benjamini and Hochberg was used for statistics.
626
627 **Figure 6. Mucin-degrading bacteria mediate fiber deprivation-induced Th1 inflammation.**
628 **A.–F.** Cytokine measurements at 60d (or earlier in SM14/FF mice that lost >20% weight) by
629 Luminex bead assay in the cecum of wild-type and *Il10*$^{-/-}$ mice colonized as adults. **G.–U.**
630 Cytokine mRNA expression in the cecum (**G.–O.**) and Mesenteric Lymph Nodes (**P.–U.** MLN)
631 of *Il10*$^{-/-}$ pups weaned to FF or FR diets (n=4-11, two-way ANOVA and post hoc test with
632 Original FDR method of Benjamini and Hochberg). Data are represented as mean ± SD. *p <
633 0.05; **p < 0.01; ***p < 0.001; ****p < 0.0001.
634
635 **Figure 7. Fiber deprivation alters IgA–bacteria interactions. A.** Concentrations of free IgA in
636 the cecal contents and feces of GF and colonized *Il10*$^{-/-}$ mice (n=4–9). **B.** Percentages of total
637 IgA-coated bacteria in the feces of FR- and FF-fed, SM14-colonized mice at 21, 56 and 79 dpw
638 (n=5–13). **C.** Percentages of total IgA-coated bacteria in the feces of SM10-, SM14- or SPF-
639 colonized *Il10*$^{-/-}$ mice and SM14-colonized WT mice fed the FR or the FF diet for 79 days (n=5–
640 8). **D.** IgA-coating profiles of fecal bacteria from SM14-colonized mice fed a FR (left) or a FF
641 (right) diet for 56 days showing the gating strategy of populations being low-coated (IgA^{low}) and
642 high-coated (IgA^{high}). Total IgA coating consists of the addition of IgA^{high} and IgA^{low} coating. **E–**
643 **F.** Percentages of IgA^{low}- (**E.**) and IgA^{high}- (**F.**) coated bacteria in the feces of indicated groups at
644 79 dpw (n=5–8). **G.** IgA-coating index (Kau index) of fecal bacteria from SM14-colonized *Il10*$^{-/-}$
645 and WT mice (n=2–5, multiple unpaired t-test and post hoc test with the two-stage linear step-up
646 procedure of Benjamini, Krieger and Yekutieli). Data are represented as mean ± SD. *p < 0.05;
647 **p < 0.01; ***p < 0.001; ****p < 0.0001. In panels A., B., C., E., F., two-way ANOVA and

648 post hoc test with the two-stage linear step-up procedure of Benjamini, Krieger and Yekutieli
649 was used for statistics.
650
651 **Supplemental Figure Legends**
652
653 **Supplemental Figure 1. Low fiber and microbiome driven inflammation development in**
654 ***Il10*$^{-/-}$ mice. A.-C.** Representative histology from wild-type (WT) SM14-colonized mice fed FR
655 (A.), WT SM14-colonized mice fed FF (B.) or WT germfree mice fed FF (C.). All pictures are
656 shown at 4x magnification, bars 500µM. **D.** Endpoint weights of the mice shown in Figure 1A
657 main text. Bold horizontal bar represents the mean and lighter error bars the S.E.M. (n=7–20)
658 **E.–F.** Relative abundance plots of SM14 bacteria in *Il10*$^{-/-}$ (E.) or wild-type (F.) mice shifted to
659 the FF diet at 14d after colonization. Dots below the graph indicate the time points at which feces
660 was sampled and the black bar on the x-axis represents the period of FR feeding. **G.** Comparison
661 of cecal *E. coli* and *B. thetaiotaomicron* populations in *Il10*$^{-/-}$ vs WT mice after 60d of
662 colonization. Bold horizontal bar represents the mean and lighter error bars the S.E.M. (n=8-9,
663 one-tailed Student's t-test and Wilcoxon test). **H.–I.** Representative staining and imaging for
664 Muc2 (green) in colonic sections from FR (H.) or FF (I.) and counter-stained with DAPI (blue).
665 These images were used for automated mucus measurement using BacSpace software[14] as
666 described in methods. **J.** Automated mucus thickness measurements generated from colonic
667 section images like those shown in H.–I. (n=5, one-tailed Student's t-test and Wilcoxon test).
668 Five mice were measured per treatment, with a total of 1–2 fecal mass sections imaged per
669 mouse. **K.** Averaged Muc2 staining intensity measurements for the mice represented in H.-J. as a
670 function of distance from the epithelium. **L.–M.** Representative visualization of 1 um-sized
671 beads (in red) layered on the distal colon epithelium (in green) after feeding FR (L.) or FF (M.)
672 to SM14-colonized *Il10*$^{-/-}$ mice. The space between the beads and epithelial cells represents the
673 penetrability of the mucus layer. **N.** Representative SM14 composition in adult mice fed FR at
674 13d post gavage (p.g.) compared to still suckling pups at 14d post birth (p.b.) and 100d old
675 SM14 colonized pups that were weaned onto either FR or FF diets. **O.** Survival plot of SM14 or
676 SPF colonized pups weaned onto FR or FF diets and maintained for a total of 100d, the typical
677 experiment duration. **P.** Cecal histology scores for SM14 or SPF colonized pups weaned onto FR
678 or FF diets and maintained for a total of 100d. P. Cecal histology scores for SM14 or SPF
679 colonized pups weaned onto FR or FF diets. Bold horizontal bar represents the mean and lighter

error bars the S.E.M. (n=5–12). In panels D, P, two-way ANOVA and post hoc test with Original FDR method of Benjamini and Hochberg was used for statistics. Related to main text **Figure 1**.

Supplemental Figure 2. Fiber supplementation reduces inflammation severity. A. Endpoint weights of mice fed variations of the FF diet with glucose replaced by fiber from apple, oat or wheat, or soluble starch. Fiber or starch were added at the concentrations listed below each treatment and an equal amount of glucose was omitted. Bold horizontal bar represents the mean and lighter error bars the S.E.M. (n=5–20). **B.** Cecal histology scores of the treatment groups shown in A. (n=5–20). **C.–F.** Relative abundance plots of the SM14 bacteria in *Il10*$^{-/-}$ mice fed fiber-enriched versions of the FF diet and containing either no added fiber (C.) or purified fiber from apple (D.), oat (E.) or wheat (F.). Relative abundance values for *A. muciniphila*, *B. caccae* and *B. ovatus* are shown next to each plot. **G.** Relative abundance comparison of all 4 mucin degraders compared to the fiber-degrader *B. ovatus* in adult mice colonized with SM14 and fed FF or the fiber supplemented diets. Note that the apple diet which had the lowest inflammation had the largest increase in *B. ovatus* and the largest decrease in mucin degrading bacteria (n=5–8). **H.** Weight trajectories of the mice that were returned to the FR diet at either 30d or 40d. **I.** Representative mucus staining for SM10 colonized mice used to measure thickness with Bacspace software. α-Muc2: green, DAPI: blue, prediction of epithelium/mucus interface: teal. **J.-O.** Relative abundance plots of the SM14 bacterial members in *Il10*$^{-/-}$ mice with all bacteria present (J.), SM10 (K.), SM10 + *A. muciniphila* (L.), SM10 + *B. caccae* (M.), SM10 + *B. thetaiotaomicron* (N.), SM10 + *B. intestinihominis* (O.). In panels A, B, G, two-way ANOVA and post hoc test with Original FDR method of Benjamini and Hochberg was used for statistics. Related to main text **Figures 1 and 2**.

Supplemental Figure 3. Effects of co-housing SM14 and SPF mice fed FR and FF diets. A.-I. 16S rRNA gene based measurements of the remaining SM14 bacteria in co-housed mice: *R. intestinalis* (**A.**), *B. thetaiotaomicron* (**B.**), *B. caccae* (**C.**), *C. aerofaciens* (**D.**), *B. uniformis* (**E.**), *M. formatexigens* (**F.**), *B. ovatus* (***G.***), *C. symbiosum* (**H.**) and *D. piger* (**I.**). **J.** PCR analysis using *E. coli* HS specific primers[13] for the presence of *E. coli* HS in mice that were mock gavaged weekly with PBS (left) or *E. coli* HS (right). **K.** Cecal LCN2 measurements in SPF mice that were gavaged weekly with *E. coli* HS and fed the FF diet. (n=6-7, one-tailed Student's t-test and Wilcoxon test). Related to main text **Figure 3**.

712

713 **Supplemental Figure 4. Fiber deprivation does not cause colitis in the absence of genetic**
714 **predisposition (WT mice) or microbiota (germfree). A.** Gating Strategy for the analysis of T
715 cells and NK cells in the cecal and colonic lamina propria. **B.-I.** Proportions of immune cell
716 populations in the cecum and colon of GF *Il10*$^{-/-}$ mice and SM14- or SM10-colonized WT mice
717 in the cell types listed on the y-axis of each panel (n=5–9, two-way ANOVA and post hoc test
718 with Original FDR method of Benjamini and Hochberg). Data are represented as mean ± SD
719 and. For each cell population, data were analyzed along with data from Fig. 3 and S5. *p < 0.05;
720 **p < 0.01; ***p < 0.001; ****p < 0.0001. Related to main text **Figure 5**.

721

722 **Supplemental Figure 5. Mucin-degrading bacteria promote Th1 immune responses in a**
723 **diet-dependent manner. A–F.** Proportion of CD3^{+} (**A.**), Th2 (**B.**), Treg cells (**C.**), Tbet^{+} Treg
724 (**D.**), RORyt^{+} Treg (**E.**) and Gata3^{+} Treg (**F.**) cells among CD45^{+} cells in the cecum and colon of
725 SM10- and SM14-colonized *Il10*$^{-/-}$ mice (n=4–11). Data are represented as mean ± SD. *p <
726 0.05; **p < 0.01; ***p < 0.001; ****p < 0.0001. In panels B–G, two-way ANOVA and post hoc
727 test with Original FDR method of Benjamini and Hochberg was used for statistics. Related to
728 main text **Figures 5-6**.

729

730 **Supplemental Figure 6. Fiber deprivation alters Ig–producing cell populations. A.–D.**
731 Proportion of plasma cells (**A.**), IgA-producing cells (**B.**), B cells (**C.**) and IgG-producing cells
732 (**D.**) among CD3^{-}CD45^{+} cells in the cecum and colon of GF, SM10- and SM14-colonized *Il10*$^{-/-}$
733 and WT mice (n=4–11, two-way ANOVA and post hoc test with Original FDR method of
734 Benjamini and Hochberg). Related to main text **Figure 7**.

735

736 **Supplemental Figure 7. Fiber deprivation alters IgA–bacteria interactions. A.** Percentages
737 of total IgA-coated bacteria as shown in the feces of SM10-, SM14- or SPF-colonized *Il10*$^{-/-}$
738 mice and SM14-colonized WT mice fed the FR or the FF diet for 21 days (n=5–8, two-way
739 ANOVA and post hoc test with the two-stage linear step-up procedure of Benjamini, Krieger and
740 Yekutieli). **B–C.** Percentages of IgA^{low}- and IgA^{high}-coated bacteria in the feces SM14-colonized
741 *Il10*$^{-/-}$ mice over time (B.) or indicated groups at 21 dpw (C.) (n=5–8, two-way ANOVA and post
742 hoc test with the two-stage linear step-up procedure of Benjamini, Krieger and Yekutieli). **D.**
743 Percentages of total (left), IgA^{low} (middle) and IgA^{high} (right) -coated bacteria in the feces of

744 SM14-colonized *Il10*$^{-/-}$ mice fed the FR, FF or EEN diet for 21 or 79 days (n=3–5, two-way
745 ANOVA and post hoc test with the two-stage linear step-up procedure of Benjamini, Krieger and
746 Yekutieli). **E.** IgA-coating index (Kau index) of fecal bacteria from SM14-colonized *Il10*$^{-/-}$ and
747 WT mice (n=2–5, multiple unpaired t-test and post hoc test with the two-stage linear step-up
748 procedure of Benjamini, Krieger and Yekutieli). Data are represented as mean ± SD. *$p < 0.05$;
749 **$p < 0.01$; ***$p < 0.001$; ****$p < 0.0001$. Related to main text **Figure 7**.

References

1 Shan, Y., Lee, M. & Chang, E. B. The Gut Microbiome and Inflammatory Bowel Diseases. *Annu Rev Med*, doi:10.1146/annurev-med-042320-021020 (2021).

2 Mirkov, M. U., Verstockt, B. & Cleynen, I. Genetics of inflammatory bowel disease: beyond NOD2. *Lancet Gastroenterol Hepatol* **2**, 224-234, doi:10.1016/S2468-1253(16)30111-X (2017).

3 Maloy, K. J. & Powrie, F. Intestinal homeostasis and its breakdown in inflammatory bowel disease. *Nature* **474**, 298-306, doi:10.1038/nature10208 (2011).

4 Ng, S. C. *et al.* Worldwide incidence and prevalence of inflammatory bowel disease in the 21st century: a systematic review of population-based studies. *Lancet* **390**, 2769-2778, doi:10.1016/S0140-6736(17)32448-0 (2017).

5 Agrawal, M., Burisch, J., Colombel, J. F. & S, C. S. Viewpoint: Inflammatory Bowel Diseases Among Immigrants From Low- to High-Incidence Countries: Opportunities and Considerations. *Journal of Crohn's & colitis* **14**, 267-273, doi:10.1093/ecco-jcc/jjz139 (2020).

6 Liu, X., Wu, Y., Li, F. & Zhang, D. Dietary fiber intake reduces risk of inflammatory bowel disease: result from a meta-analysis. *Nutrition research (New York, N.Y* **35**, 753-758, doi:10.1016/j.nutres.2015.05.021 (2015).

7 Chassaing, B. *et al.* Dietary emulsifiers impact the mouse gut microbiota promoting colitis and metabolic syndrome. *Nature* **519**, 92-96, doi:10.1038/nature14232 (2015).

8 Chassaing, B. *et al.* Randomized Controlled-Feeding Study of Dietary Emulsifier Carboxymethylcellulose Reveals Detrimental Impacts on the Gut Microbiota and Metabolome. *Gastroenterology* **162**, 743-756, doi:10.1053/j.gastro.2021.11.006 (2022).

9 Khan, S. *et al.* Dietary simple sugars alter microbial ecology in the gut and promote colitis in mice. *Science translational medicine* **12**, doi:10.1126/scitranslmed.aay6218 (2020).

10 David, L. A. *et al.* Diet rapidly and reproducibly alters the human gut microbiome. *Nature* **505**, 559-563, doi:10.1038/nature12820 (2014).

11 Porter, N. T. & Martens, E. C. The Critical Roles of Polysaccharides in Gut Microbial Ecology and Physiology. *Annual review of microbiology* **71**, 349-369, doi:10.1146/annurev-micro-102215-095316 (2017).

12 Perler, B. K., Friedman, E. S. & Wu, G. D. The Role of the Gut Microbiota in the Relationship Between Diet and Human Health. *Annu Rev Physiol*, doi:10.1146/annurev-physiol-031522-092054 (2022).

13 Desai, M. S. *et al.* A Dietary Fiber-Deprived Gut Microbiota Degrades the Colonic Mucus Barrier and Enhances Pathogen Susceptibility. *Cell* **167**, 1339-1353 e1321, doi:10.1016/j.cell.2016.10.043 (2016).

14 Earle, K. A. *et al.* Quantitative Imaging of Gut Microbiota Spatial Organization. *Cell Host Microbe* **18**, 478-488, doi:10.1016/j.chom.2015.09.002 (2015).

15 Parrish, A. *et al.* Akkermansia muciniphila exacerbates food allergy in fibre-deprived mice. *Nat Microbiol* **8**, 1863-1879, doi:10.1038/s41564-023-01464-1 (2023).

16 Neumann, M. *et al.* Deprivation of dietary fiber in specific-pathogen-free mice promotes susceptibility to the intestinal mucosal pathogen Citrobacter rodentium. *Gut microbes* **13**, 1966263, doi:10.1080/19490976.2021.1966263 (2021).

17 Schroeder, B. O. *et al.* Bifidobacteria or Fiber Protects against Diet-Induced Microbiota-Mediated Colonic Mucus Deterioration. *Cell Host Microbe* **23**, 27-40 e27, doi:10.1016/j.chom.2017.11.004 (2018).

18 Zhu, L. *et al.* IL-10 and IL-10 Receptor Mutations in Very Early Onset Inflammatory Bowel Disease. *Gastroenterology research* **10**, 65-69, doi:10.14740/gr740w (2017).
19 Keubler, L. M., Buettner, M., Hager, C. & Bleich, A. A Multihit Model: Colitis Lessons from the Interleukin-10-deficient Mouse. *Inflamm Bowel Dis* **21**, 1967-1975, doi:10.1097/MIB.0000000000000468 (2015).
20 Sellon, R. K. *et al.* Resident enteric bacteria are necessary for development of spontaneous colitis and immune system activation in interleukin-10-deficient mice. *Infect Immun* **66**, 5224-5231 (1998).
21 Gustafsson, J. K. *et al.* An ex vivo method for studying mucus formation, properties, and thickness in human colonic biopsies and mouse small and large intestinal explants. *American journal of physiology. Gastrointestinal and liver physiology* **302**, G430-438, doi:10.1152/ajpgi.00405.2011.
10.1152/ajpgi.00405.2011 (2012).
22 Marcobal, A. *et al.* Bacteroides in the Infant Gut Consume Milk Oligosaccharides via Mucus-Utilization Pathways. *Cell Host Microbe*, doi:10.1016/j.chom.2011.10.007 (2011).
23 Martens, E. C. *et al.* Recognition and Degradation of Plant Cell Wall Polysaccharides by Two Human Gut Symbionts. *Plos Biol* **9**, doi:10.1371/journal.pbio.1001221 (2011).
24 Furter, M., Sellin, M. E., Hansson, G. C. & Hardt, W. D. Mucus Architecture and Near-Surface Swimming Affect Distinct Salmonella Typhimurium Infection Patterns along the Murine Intestinal Tract. *Cell reports* **27**, 2665-2678 e2663, doi:10.1016/j.celrep.2019.04.106 (2019).
25 Logan, M. *et al.* Analysis of 61 exclusive enteral nutrition formulas used in the management of active Crohn's disease-new insights into dietary disease triggers. *Aliment Pharmacol Ther* **51**, 935-947, doi:10.1111/apt.15695 (2020).
26 Day, A. S. & Lopez, R. N. Exclusive enteral nutrition in children with Crohn's disease. *World J Gastroenterol* **21**, 6809-6816, doi:10.3748/wjg.v21.i22.6809 (2015).
27 Guo, C. J. *et al.* Depletion of microbiome-derived molecules in the host using Clostridium genetics. *Science* **366**, doi:10.1126/science.aav1282 (2019).
28 Gorissen, S. H. M. *et al.* Protein content and amino acid composition of commercially available plant-based protein isolates. *Amino acids* **50**, 1685-1695, doi:10.1007/s00726-018-2640-5 (2018).
29 Barros, L., Ferreira, C. & Veldhoen, M. The fellowship of regulatory and tissue-resident memory cells. *Mucosal immunology* **15**, 64-73, doi:10.1038/s41385-021-00456-w (2022).
30 Yang, B. H. *et al.* Foxp3(+) T cells expressing RORgammat represent a stable regulatory T-cell effector lineage with enhanced suppressive capacity during intestinal inflammation. *Mucosal immunology* **9**, 444-457, doi:10.1038/mi.2015.74 (2016).
31 Wang, Y., Su, M. A. & Wan, Y. Y. An essential role of the transcription factor GATA-3 for the function of regulatory T cells. *Immunity* **35**, 337-348, doi:10.1016/j.immuni.2011.08.012 (2011).
32 Wohlfert, E. A. *et al.* GATA3 controls Foxp3(+) regulatory T cell fate during inflammation in mice. *J Clin Invest* **121**, 4503-4515, doi:10.1172/JCI57456 (2011).
33 Gomes-Santos, A. C. *et al.* New insights into the immunological changes in IL-10-deficient mice during the course of spontaneous inflammation in the gut mucosa. *Clin Dev Immunol* **2012**, 560817, doi:10.1155/2012/560817 (2012).
34 Tan, J. *et al.* Dietary Fiber and Bacterial SCFA Enhance Oral Tolerance and Protect against Food Allergy through Diverse Cellular Pathways. *Cell reports* **15**, 2809-2824, doi:10.1016/j.celrep.2016.05.047 (2016).

35 Castro-Dopico, T. *et al.* Anti-commensal IgG Drives Intestinal Inflammation and Type 17 Immunity in Ulcerative Colitis. *Immunity* **50**, 1099-1114 e1010, doi:10.1016/j.immuni.2019.02.006 (2019).
36 Palm, N. W. *et al.* Immunoglobulin A coating identifies colitogenic bacteria in inflammatory bowel disease. *Cell* **158**, 1000-1010, doi:10.1016/j.cell.2014.08.006 (2014).
37 Caruso, R. *et al.* A specific gene-microbe interaction drives the development of Crohn's disease-like colitis in mice. *Sci Immunol* **4**, doi:10.1126/sciimmunol.aaw4341 (2019).
38 Pizarro, T. T. *et al.* SAMP1/YitFc mouse strain: a spontaneous model of Crohn's disease-like ileitis. *Inflamm Bowel Dis* **17**, 2566-2584, doi:10.1002/ibd.21638 (2011).
39 Taurog, J. D. *et al.* Inflammatory disease in HLA-B27 transgenic rats. *Immunol Rev* **169**, 209-223, doi:10.1111/j.1600-065x.1999.tb01317.x (1999).
40 Kakade, M. L. *et al.* Failure of soybean trypsin inhibitor to exert deleterious effects in calves. *Journal of dairy science* **59**, 1484-1489, doi:10.3168/jds.S0022-0302(76)84388-3 (1976).
41 Packey, C. D. & Sartor, R. B. Commensal bacteria, traditional and opportunistic pathogens, dysbiosis and bacterial killing in inflammatory bowel diseases. *Current opinion in infectious diseases* **22**, 292-301 (2009).
42 Pudlo, N. A. *et al.* Phenotypic and Genomic Diversification in Complex Carbohydrate-Degrading Human Gut Bacteria. *mSystems* **7**, e0094721, doi:10.1128/msystems.00947-21 (2022).
43 Steimle, A. *et al.* Constructing a gnotobiotic mouse model with a synthetic human gut microbiome to study host-microbe cross talk. *STAR Protoc* **2**, 100607, doi:10.1016/j.xpro.2021.100607 (2021).
44 Han, J., Lin, K., Sequeira, C. & Borchers, C. H. An isotope-labeled chemical derivatization method for the quantitation of short-chain fatty acids in human feces by liquid chromatography-tandem mass spectrometry. *Anal Chim Acta* **854**, 86-94, doi:10.1016/j.aca.2014.11.015 (2015).
45 Meira, L. B. *et al.* DNA damage induced by chronic inflammation contributes to colon carcinogenesis in mice. *J Clin Invest* **118**, 2516-2525, doi:10.1172/JCI35073 (2008).
46 Kozich, J. J., Westcott, S. L., Baxter, N. T., Highlander, S. K. & Schloss, P. D. Development of a dual-index sequencing strategy and curation pipeline for analyzing amplicon sequence data on the MiSeq Illumina sequencing platform. *Appl Environ Microbiol* **79**, 5112-5120, doi:10.1128/AEM.01043-13 (2013).
47 Schloss, P. D. *et al.* Introducing mothur: open-source, platform-independent, community-supported software for describing and comparing microbial communities. *Appl Environ Microbiol* **75**, 7537-7541, doi:10.1128/AEM.01541-09 (2009).

890 ## STAR METHODS

891

892 **Key resources table**

REAGENT or RESOURCE	SOURCE	IDENTIFIER
Antibodies		
eF450-conjugated anti-mouse B220/CD45R (RA3-6B2)	eBiosciences	Cat#48-0452-82
BV650-conjugated anti-mouse B220/CD45R (RA3-6B2)	BD	Cat#563893
APC-conjugated anti-mouse CD138 (281-2)	Biolegend	Cat#142506
eF506-conjugated anti-mouse CD19 (1D3)	eBiosciences	Cat#69-0193-82
BV711-conjugated anti-mouse CD3 (17A2)	Biolegend	Cat#100241
FITC-conjugated anti-mouse CD335/NKp46 (29A1.4)	Biolegend	Cat#137606
BV605-conjugated anti-mouse CD4 (RM4-5)	Biolegend	Cat#100548
BV780-conjugated anti-mouse CD45 (30-F11)	BD	Cat#564225
PE-Cy5-conjugated anti-mouse CD8 (53-6.7)	Biolegend	Cat#100710
PE-eF610-conjugated anti-mouse EOMES (Dan11mag)	eBiosciences	Cat#61-4875-82
eF450-conjugated anti-mouse FoxP3 (FJK-16s)	eBiosciences	Cat#48-5773-82
PE-conjugated anti-mouse GATA3 (16E10A23)	Biolegend	Cat#653804
FITC-conjugated anti-mouse IgA (mA-6E1)	eBiosciences	Cat#11-4204-83
FITC-conjugated anti-mouse IgA (polyclonal)	Southern Biotech	Cat#1040-02
PerCP-Cy5.5-conjugated anti-mouse IgD (11-26c.2a)	Biolegend	Cat#405710
PE-conjugated anti-mouse IgE (RME-1)	Biolegend	Cat#406908
PE-Cy7 -conjugated anti-mouse IgG (Poly4053)	Biolegend	Cat#405315
PE-Cy5-conjugated anti-mouse IgM (R6-60.2)	BD	Cat#553409
APC-conjugated anti-mouse RORgt (AFKJS-9)	eBiosciences	Cat#17-6988-82
PE-Cy7 -conjugated anti-mouse Tbet (4B10)	Biolegend	Cat#644824
rabbit anti-mouse IgA	Novus Biologicals, Bio-Techne	Cat#NB7506
mouse IgA Isotype Control UNLB	Southern Biotech	Cat#0106-01
Phosphatase Alkaline-conjugated goat anti-mouse IgA	Southern Biotech	Cat#1040-04
phosphate tablet	Sigma	Cat#S0642-200 TAB
Fc Block (Rat anti-mouse CD16 and CD32)	BD Pharmingen	Cat#553141
anti-FITC MicroBeads	Miltenybiotec	130-048-701
Mucin 2 antibody (H-300)	Santa Cruz Biotechnology	SC-15334
Alexa Fluor 488 goat anti-rabbit IgG	Invitrogen	A11008
Bacterial and virus strains		
Akkermansia muciniphila: DMS 22959, type strain	DSMZ	Cat#DMS 22959
Bacteroides caccae: DSM 19024, type strain	DSMZ	Cat#DSM 19024
Bacteroides ovatus: DSM 1896, type strain	DSMZ	Cat#DSM 1896
Bacteroides thetaiotaomicron: DSM 2079, type strain	DSMZ	Cat#DSM 2079
Bacteroides uniformis: ATCC 8492, type strain	ATCC	Cat#ATCC 8492
Barnesiella intestinihominis: YIT11860	DSMZ	Cat#DSM 21032

Clostridium symbiosum: DSM 934, type strain, 2	DSMZ	Cat#DSM 934
Collinsella aerofaciens: DSM 3979, type strain	DSMZ	Cat#DSM 3979
Desulfovibrio piger: ATC 29098, type strain	ATCC	Cat#ATC 29098
Escherichia coli HS	ATCC	N/A
Eubacterium rectale: DSM 17629, A1-86	DSMZ	Cat#DSM 17629
Faecalibacterium prausnitzii: DSM 17677, A2-165	DSMZ	Cat#DSM 17677
Marvinbryantia formatexigens: DSM 14469, type strain, I-52	DSMZ	Cat#DSM 14469
Roseburia intestinalis: DSM 14610 type strain, L1-82	DSMZ	Cat#DSM 14610
Biological samples		
Chemicals, peptides, and recombinant proteins		
Acetic acid 100% 1l	Carl Roth	6755.1
Chloroform, 99.8+%, Certified AR for Analysis, Stabilised with Amylene, Fisher Chemical	Fisher Scientific	10122190
Méthanol 5 litres	Carl Roth	4627.6
Phenol/Chloroform/Isoamyl Alcohol (125:24:1 Mixture, pH 4.3, Liq.), Fisher BioReagents	Fisher Scientific	10699543
Sodium chloride, 1 kg, ≥99,5 %, p.a., ACS, ISO	Carl Roth	3957.1
TRIS, 1 kg, PUFFERAN® ≥99,9 %, p.a.	Carl Roth	4855.2
Ethylenediamine tetraacetic acid disodium salt dihydrate, 1 kg	Carl roth	X986.2
Sodium Dodecyl-Sulfate	Fisher Scientific	BP166
Isopropanol, Extra Pure, SLR, Fisher Chemical	Fisher Scientific	10477070
Ethanol	VWR	1.08543.0250
RNA Stabilization Reagent (250 ml)	QIAGEN	76106
RNAprotect	QIAGEN	76506
TRIzol™ Reagent	Ambion / Fisher Scientific	15596018
carbonate-bicarbonate buffer	Sigma	C3041
Invitrogen™ Random primers (Invitrogen™ 48190011)	Fisher Scientific	10646313
Thermo Scientific™ DNase I, RNase-free (Thermo Scientific™ EN0521)	Fisher Scientific	10649890
Invitrogen™ SuperScript™ IV Reverse Transcriptase	Fisher Scientific	15317696
Invitrogen™ Platinum™ Taq DNA Polymerase	Fisher Scientific	10358742
Invitrogen™ Eau distillée exempte de DNase / RNase UltraPure™	Fisher Scientific	12060346
Invitrogen™ SYBR™ Green I Nucleic Acid Gel Stain, 10,000X concentrate in DMSO	FisherScientific	10710004
Invitrogen™ dNTP Set (100 mM) Solution	Fisher Scientific	10083252
Invitrogen™ RNaseOUT™ Recombinant Ribonuclease Inhibitor	Fisher Scientific	10154652
Tween-20	Sigma	P1379
Trisma-base	Sigma	T1503
Trizma-Acetate	Sigma	T1258

Potassium chloride, CELLPURE® ≥99 %	Carl Roth	HN02.2
Bovine Serum Albumin	Sigma	A9647
Zombie NIR™ Fixable Viability dye	BioLegend	423105
fetal bovine serum	Gibco	10500 - 064
Magnesium chloride (MgCl2.6H2O)	Sigma	M9272
Normal Goat Serum	Imtec Diagnostics	0060-01
Gibco™ Goat Serum, New Zealand origin	Fisher	11540526
HEPES Buffer, 1M stock in normal saline, 100 ml	Westburg	LO BE17-737E
SYTO™ 60 Red Fluorescent Nucleic Acid Stain	Invitrogen	S11342
paraformaldehyde	Sigma	441244
paraffin	Sigma	18512
Xylenes, ≥98.5%, ACS Reagent, xylenes plus ethylbenzene basis, Honeywell™ Riedel-de Haën™	FisherScientific	15692690
Sodium citrate	Fisher	S279
Invitrogen™ ProLong™ Gold Antifade Mountant with DAPI, P36931	FisherScientific	11549306
Invitrogen™ SYTO™ 9 Green Fluorescent Nucleic Acid Stain	Fisher Scientific	10237582
Sodium chloride, 1 kg, ≥99,5 %, p.a., ACS, ISO	Carl Roth	3957.1
Potassium chloride, CELLPURE® ≥99 %	Carl Roth	HN02.2
Potassium Phosphate, Monobasic	Carl Roth	P018.1
Sodium acetate trihydrate, 500 g	Carl roth	HN05.1
Magnesium sulfate	Carl Roth	P027.1
Calcium chloride dihydrate	Carl Roth	HN04.2
Pyruvic acid sodium salt, 25 g	Carl roth	8793.1
L-Glutamic acid, 25 g	Carl roth	1743.1
Sodium hydrogen carbonate, 1 kg	Carl roth	HN01.2
ethylenediaminetetraacetic acid	Sigma	EDS
Volatile Free Acid Mix	Sigma	CRM46975
3C-Short Chain Fatty Acids Stool Mixture	Sigma	SBR00035-1mL
3-Nitrophenylhydrazine hydrochloride	Sigma	N21804
EDAC Hydrochloride	Sigma	341006
HPLC grade pyridine	Sigma	270407
LC–MS grade acetonitrile	Sigma	34851
LC–MS grade water	Sigma	270733
LC–MS grade formic acid	Sigma	5438040450
Critical commercial assays		
DNeasy Blood & Tissue kit	QIAGEN	69506
Buffer ATL (200 ml)	QIAGEN	19076
Qiagen proteinase K (10 ml)	QIAGEN	19133
RNeasy Mini kit	QIAGEN	74106
DuoSet mouse lipocalin-2/NGAL ELISA kit	R&D Biosystems	DY1857
ZymoBIOMICS Microbial Community DNA Standard	Zymo Research	D6306

Lamina Propria Dissociation Kit	Miltenyi Biotec	130-097-410
FOXP3/Transcription Factor Staining Buffer kit	eBioscences	Cat#00-5523-00
BD Cytofix/CytopermTM Fixation/Permeabilization Solution Kit	BD Biosciences	Cat#554714
Deposited data		
Experimental models: Cell lines		
Experimental models: Organisms/strains		
Mice B6.129P2-Il10tm1Cgn/JZtm	Institut für Versuchstierkunde und Zentrales Tierlaboratorium	N/A
Mice wild-type C57BL/6J	Germ-Free Mouse Facility – University of Michigan and University of Bern	N/A
Mice C57BL/6J Muc2$^{-/-}$	Albert Einstein University	N/A
Mice C57BL/6J IL10$^{-/-}$ Muc2$^{-/-}$	This study	N/A
Mice C57BL/6J IL10$^{-/-}$	Germ-Free Mouse Facility – University of Michigan	N/A
Oligonucleotides		
Cytokine *Il5* Forward	TGAGGCTTCCTGTCCCTACT	Eurogentec
Cytokine *Il5* Reverse	CCACACTTCTCTTTTTGGCGG	Eurogentec
Cytokine *Il6* Forward	TAGTCCTTCCTACCCCAATTTCC	Eurogentec
Cytokine *Il6* Reverse	TTGGTCCTTAGCCACTCCTTC	Eurogentec
Cytokine *Il10* Forward	CTGCCTGCTCTTACTGACTGG	Eurogentec
Cytokine *Il10* Reverse	TGGGAAGTGGGTGCAGTTATT	Eurogentec
Cytokine *Il12p40* Forward	TGTGGAATGGCGTCTCTGTC	Eurogentec
Cytokine *Il12p40* Reverse	GCCTTTGCATTGGACTTCGG	Eurogentec
Cytokine *Il13* Forward	CCTGGCTCTTGCTTGCCTT	Eurogentec
Cytokine *Il13* Reverse	GGTCTTGTGTGATGTTGCTCA	Eurogentec
Cytokine *Il17f* Forward	GGTAGCAGCTCGGAAGAACC	Eurogentec
Cytokine *Il17f* Reverse	TGGAATTCACGTGGGACAGA	Eurogentec
Cytokine *Il22* Forward	TCGTCAACCGCACCTTTATG	Eurogentec
Cytokine *Il22* Reverse	CCCGATGAGCCGGACA	Eurogentec
Cytokine *Il23* Forward	TGGAGCAACTTCACACCTCC	Eurogentec

Cytokine *Il23* Reverse	GGGCAGCTATGGCCAAAAAG	Eurogentec
Cytokine *Il33* Forward	CGTTCTGGCCTCACCATAAGA	Eurogentec
Cytokine *Il33* Reverse	CCGTGGATAGGCAGAGAAGT	Eurogentec
Cytokine *Ifng* Forward	ATGAACGCTACACACTGCATC	Eurogentec
Cytokine *Ifng* Reverse	CCATCCTTTTGCCAGTTCCTC	Eurogentec
Cytokine *Tnfa* Forward	AGCCCACGTCGTAGCAAAC	Eurogentec
Cytokine *Tnfa* Reverse	GATAGCAAATCGGCTGACGG	Eurogentec
Cytokine *Tgfb* Forward	TGATACGCCTGAGTGGCTGTCT	Eurogentec
Cytokine *Tgfb* Reverse	CACAAGAGCAGTGAGCGCTGAA	Eurogentec
Hsp90 Forward	CAGAAGGCTGAGGCAGACAA	Eurogentec
Hsp90 Reverse	ATCATGCGGTAGATGCGGTT	Eurogentec
Synthetic microbiota 14 species primers	N/A	
Recombinant DNA		
Software and algorithms		
SoftMax Pro 7 Software	Molecular Devices	N/A
FlowJo	BD Biosciences	N/A
BacSpace	***Earle et al., 2015***	N/A
Zen 3.0	Carl Zeiss Microscopy GmbH	N/A
mothur v1.42.3	***Schloss et al., 2009***	N/A
Imaris	Oxford Instruments Imaris	N/A
Agilent Masshunter Workstation Software LC/MS Data Acquisition for 6400 Series Triple Quadrupole MS with Version B.08.02	Agilent Technologies	N/A
Other		
Acid-washed glass beads (212-300 mm)	Sigma-Aldrich	Cat#G1277
Anaerobic chamber	Coy manufacturing	Vinyl Type A + Type B
Nunc® MaxiSorp™ 384 well plates	Thermo Scientific	464718
SpectraMax Plus 384 Microplate Reader	Molecular Devices	ABS PLUS
gentleMACS Dissociators	Miltenyi Biotec	130-096-427
NovoCyte Quanteon Flow Cytometer Systems 4 Lasers	ACEA Biosciences / Agilent	2010097
70 µm straining sieve	Clear Line	141379C
QuadroMACS™ Separator	Miltenyi Biotec	130-090-976
LS column	Miltenyi Biotec	130-042-401
Zeiss Apotome	Zeiss	Discontinued

Microscope Axio Examiner KMAT	Carl Zeiss Microscopy GmbH	491406-9880-010
Perfusion chambers for bead assay	Gustafsson et al., 2012	N/A
FluoSphere™ carboxylate beads, 1µm, red 580/605	Invitrogen	F8821
Screw cap tube, 1.5ml, non-skirted, sterile, white cap	Greiner	716261
Microtube, PP, 2ml, screw cap, 5x50pc, S	Greiner	723261
Stainless Steel Beads, 5 mm (200)	Qiagen	69989
White PCR plates (25 pcs)	Bioplastics	AB70659
RETSCH Broyeur mélangeur MM 400 (Tissue Lyser)	Fisher Scientific	10573034
Retsch™ Rack d'adaptateur en PTFE	Fisher Scientific	10122852
CFX96TM RealTime System (C1000 Thermal Cycler)	Biorad	1855195
Implen™ NanoPhotometer™ N60 Micro-Volume UV-VIS Spectrophotometer (N60-Touch)	Fisher Scientific	15442203
Agilent Technologies Triple Quad 6470 LC/MS system consist of 1290 Infinity II LC Flexible Pump (Quaternary Pump)	Agilent Technologies	Reference
1290 Infinity II Multisampler, 1290 Infinity II Multicolumn Thermostat with 6 port valve and 6470 triple quad mass spectrometer	Agilent Technologies	Reference
Waters Acquity UPLC BEH TSS C18 column (2.1 x 100mm, 1.7µm) column	Waters	

LEAD CONTACT AND MATERIALS AVAILABILITY

Bacterial strains and data associated with this study are available to interested parties upon request to emartens@umich.edu.

EXPERIMENTAL MODEL AND SUBJECT DETAILS

Animal models, colonization diet and sample processing

Animal experiments at the University of Michigan followed protocols approved by the University of Michigan Institutional Animal Care and Use Committee (IACUC) and were supervised by licensed verterinarians. Germ-free B6.129P2-Il10tm1Cgn/JZtm mice (Institut für Versuchstierkunde und Zentrales Tierlaboratorium, Hannover, Germany) and wild-type C57BL/6J (University of Bern, Switzerland) were bred at the animal facility of the University of Luxembourg and underwent protocols approved by the Animal Experimentation Ethics Committee of the University of Luxembourg and the Ministre de l'Agriculture, de la Viticulture et du Development rural du Grand-Duché du Luxembourg (LUPA 2020/20). Germfree males

908 and females were colonized at 7–10 weeks of age and none of these mice was involved in any
909 previous experiments/treatments. Mice were either housed alone or in groups of appropriate
910 gender, litter, and dietary experiments. Food and autoclaved distilled water were provided ad
911 libitum. Mice were weighed and monitored at least weekly for diarrhea, prolapses, and general
912 health state and this was increased to daily monitoring in animals that began experiencing weight
913 loss. The *Muc2*$^{-/-}$ mice, crossed to C57BL/6J background, were obtained from Leonard
914 Augenlicht (Albert Einstein University). For the generation of *Il10*$^{-/-}$ *Muc2*$^{-/-}$ double knockout
915 (DKO), the single KO mice were crossed to obtain double heterozygous mice until generation of
916 *Il10*$^{-/-}$ *Muc2*$^{+/-}$. Full double KO mice developed spontaneous prolapse in germ-free condition
917 during prolonged breeding periods, thus, the *Il10*$^{-/-}$ *Muc2*$^{+/-}$ mice were used to generate the
918 double KO mice used for all experiments. Genotyping was performed by extracting DNA from
919 ear punches (Transnetyx). Mice were gavaged with the synthetic microbiota at 6–8 weeks and
920 proceeded to diet change as previously described. The synthetic microbiota bacteria were grown
921 in their respective medium[13] or a modified YCFA medium[43] prior to community assembly for
922 gavages. The bacteria were cultivated under anaerobic atmosphere maintained with a gas mixture
923 (85% N_2, 10% H_2, 5% CO_2) to an optical density (absorbance 600nm) ranging from 0.5 to 1.0.
924 The communities were assembled by mixing equal volumes of each specific bacterium and
925 aliquoted into sealed screw cap tubes with its own headspace. Each mouse was gavaged with 0.2
926 mL of its specific community, depending on the experiment, with freshly prepared inocula for
927 two-three consecutive days. A humane endpoint was used for mice that lost $\geq$20% of their
928 starting weight and these mice were counted as lethalities in the weight loss and survival curves
929 shown. Animals were euthanized using CO_2 asphyxiation for 5 minutes followed by cervical
930 dislocation. The gastrointestinal tracts were retrieved quickly, to prevent autolysis, and the
931 sections separated. Cecal and colon contents of each animal were flash frozen in liquid nitrogen
932 and kept at -80°C until further use.

933 The FR diet (Lab Diet 5013) and FF diet (Envigo-Teklad TD.130343) have been
934 previously described[13]. The EEN diet employed was Nestle Nutren 1.5, which was lyophilized
935 and sent to Envigo rodent diets to be formed into pellets, bagged and gamma irradiated prior to
936 use. Apple (Vitacel AF401), oat (Vitacel HF600-30) and wheat (Vitacel WF200) fibers were
937 from J. Rettenmaier (Schoolcraft, MI, USA) and added to the FF diet at 7.5% w/w with a
938 corresponding decrease in the amount of glucose in the FF diet. Soluble, highly digestible starch
939 was provided by Cargill (Gel Instant 12412).

940

941 **METHOD DETAILS**

942 **DNA extraction**

943 DNA from fecal and cecal samples were isolated using a bead-beating phenol:chloroform
944 extraction method followed by DNeasy Blood & Tissue Kit (QIAGEN, USA). In short, samples
945 were weighed between 10-50mg and combined with acid-washed glass beads (212-300mm;
946 Sigma-Aldrich, USA), 500uL Buffer A (200 mM NaCl, 200 mM Tris, 20 mM EDTA, 210 uL
947 SDS (20% w/v, filter-sterelized), and 500 uL phenol:chloroform (Thermo Fisher Scientific,
948 USA). The samples were disrupted using a Mini-Beadbeater-16 (Biospec Products, USA) for 3
949 minutes at room temperature and centrifuged (10,000 rpm, 4°C, 3 minutes). The aqueous phase
950 was recovered and mixed with an equal volume of phenol:chloroform by gentle inversion and
951 centrifuged (10,000 rpm, 4°C, 3 minutes). The remaining aqueous phase was recovered and
952 mixed with 500 µL of chloroform, mixed by gentle inversion, and centrifuged (10,000 rpm, 4°C,
953 3 minutes). Recovered aqueous phase was mixed with 1 volume of isopropanol and 1/10 volume
954 of 3M sodium acetate, and stored at -80°C for 20 minutes for DNA precipitation. Samples were
955 centrifuged (15000 rpm, 4°C, 20 minutes), supernatant discarded, washed with 70% ethanol, air-
956 dried, and resuspended in nuclease-free water. The sample DNA extracts were further purified
957 with DNeasy Blood & Tissue kit, following manufacturer protocol (QIAGEN).

958 **RNA extraction, reverse transcription and qPCR**

959 Freshly retrieved ileal, cecal and distal colon tissues were transferred into RNAlater™
960 (QIAGEN) and kept at 4°C up to a week. Then, RNAlater™ was removed and tissues were
961 stored at -80°C until further use. Frozen tissues were transferred into 1 mL of TRIzol reagent
962 (Invitrogen™), homogeneized with a 5 mm metal bead on a bead beater for 8 min at 30Hz and
963 centrifuged for 3 min at 13000 rpm, 4°C. The supernatant was recovered, mixed thoroughly with
964 200 µl of chloroform and incubated at room temperature for 2-3 min before a centrifigation for
965 15 min at 13000 rpm, 4°C. The aqueous phase was recovered, mixed again with an equal amount
966 of chloroform and centrifuged for 15 min at 13000 rpm, 4°C. The aqueous phase was recovered,
967 mixed by inversion with 500 µl of isopropanol, incubated for 10 min at room temperature, and
968 centrifuged for 10 min at 13000 rpm, 4°C. The pellet was washed with 1 ml Ethanol 70% and
969 centrifuged for 5 min at 10000 rpm. The supernatant was discarded and the pellet dried for 5-10
970 min at 37°C, resuspended with 50 µl nuclease-free water and incubated for 15 min at 56°C.

971 Finally, samples were treated with DNase following the Thermo Scientific DNase1, RNase-free
972 Protocol, and RNA were purified with the RNeasy Mini kit (QIAGEN) according to
973 manufacturer instructions. Final RNA concentrations were quantified by Nanodrop.

974 **Lipocalin-2 (LCN2) measurements in cecal and fecal contents**

975 Frozen cecal and fecal samples were used to quantify the presence of lipocalin-2 protein
976 (LCN2) by enzyme linked immunosorbent assay (ELISA). Samples previously frozen (cecal, -
977 80°C, and fecal, -20°C) were weighed in new tubes between 5-5 mg. Samples were kept over dry
978 ice during the weighing. Samples were resuspended in 1 mL PBS (pH 7.4), vortexed for 30s, and
979 kept at 4°C overnight to homogenize. Samples were then extensively vortexed to a homogeneous
980 solution. To measure the LCN2 levels, a DuoSet mouse lipocalin-2/NGAL ELISA kit (R&D
981 Biosystems, USA) was employed using several dilutions of sample homogeneous solution.
982 Quantification was done following manufacturer protocol.

983 **Soluble IgA measurements in cecal and fecal contents**

984 To measure soluble IgA levels, Nunc® MaxiSorp™ 384 well plates (Sigma-Aldrich)
985 were coated overnight with 10 ng/well rabbit anti-mouse IgA (Novus Biologicals, Bio-Techne
986 NB7506) in 20 µl/well of carbonate-bicarbonate buffer (Sigma, Ref.: C3041). After four washes
987 with Washing Buffer (1% Tween-20, 154mM Sodium Chloride and 10mM Trisma-base), 75µl of
988 Blocking Buffer (15 mM Trizma-Acetate, 136 mM Sodium Chloride, 2 mM Potassium Chloride
989 and 1% (w/v) BSA (Bovine Serum Albumin)). After 2h at room temperature, wells were washed
990 again. Sample homogeneous solution and standards (mouse IgA Isotype Control UNLB,
991 Southern Biotech, Imtec Diagnostics, Ref: 0106-01) were diluted in Dilution Buffer (15 mM
992 Trizma-Acetate, 136 mM Sodium Chloride, 2 mM Potassium Chloride, 0.1% (w/v) Tween-20,
993 and 1% BSA) and incubated into the plate at 20 µl/well, room temperature for 90 min. After
994 washing, 20 µl/well of a Phosphatase Alkaline-conjugated goat anti-mouse IgA (Southern
995 Biotech, Imtec diagnostics, Ref: 1040-04), diluted 1/1000 in Dilution Buffer, was added and
996 incubated at room temperature for 90 min. After a final wash, 40 µl/well of substrate (1
997 phosphate tablet (Sigma, ref S0642-200 TAB) dissolved in 10 mL Substrate Buffer (1 mM 2-
998 Amino-2-methyle-1-propanole, 0.1 mM MgCl2.6H2O)) was added. The plate was incubated at
999 37°C for 60 min before the absorbance was measured at 405 nm using an ELISA plate reader
1000 (SpectraMax Plus 384 Microplate Reader from Molecular Devices; Software: SoftMax Pro 7

1001 Software, Molecular Devices). The IgA concentration was determined for each sample using the
1002 formulated standard curve.

1003

1004 **Short- and branched-chain fatty acid quantification**

1005 Short-chain and branched-chain fatty acids (SCFAs) standards mixture was obtained
1006 from Sigma (CRM46975). 13C-short chain fatty acid stool mixture (Sigma, SBR00035-1mL)
1007 was used as the internal standard (IS). Analytical reagent-grade 3-nitrophenylhydrazine
1008 (3NPH)·HCl (Cat#N21804), EDAC·HCl (Cat#341006); HPLC grade pyridine (Cat#270407);
1009 LC–MS grade acetonitrile (Cat#34851), water (Cat#270733), and formic acid
1010 (Cat#5438040450) were also purchased from Sigma–Aldrich. The working standard solutions
1011 were created by performing serial dilution from the 10mM stock solution down to nM range
1012 using freshly prepared 50% (v/v) aqueous acetonitrile in water. The chemical derivatization
1013 protocol was modified from Han et al. [44]. Briefly, 20µL of the working standard solutions or
1014 samples was mixed with 40µL of 200mM 3NPH in 50% aqueous acetonitrile, 120mM EDAC-
1015 6% (v/v) pyridine solution in the same solvent and 4µL of the IS in a Verex glass vial. The
1016 mixture was reacted at 40°C for 30 min. After reaction, 96µL of 0.1% formic acid in 10%
1017 acetonitrile solution was added to the mixture to quench the reaction. 30µL of the reaction
1018 solution was then transferred to a new HPLC vial and 2-µL aliquot of each solution was injected
1019 into the LC- MS/MS instrument. Each modified SCFA was optimized in Agilent MS for detection
1020 through Agilent Optimizer 2.0. All optimized SCFAs information was combined, and a LC-MRM
1021 MS method was created. Retention time for each SCFA was determined from two transitions. Then
1022 the MRM MS method was transformed into a dynamic MRM MS or dMRM MS method with all the
1023 RTs and MS information for the final LC-MS/MS acquisition method.

1024 LC-MS/MS analysis was performed on the Agilent Technologies Triple Quad 6470
1025 LC/MS system consist of 1290 Infinity II LC Flexible Pump (Quaternary Pump), 1290 Infinity II
1026 Multisampler, 1290 Infinity II Multicolumn Thermostat with 6 port valve and 6470 triple quad
1027 mass spectrometer. Agilent Masshunter Workstation Software LC/MS Data Acquisition for
1028 6400 Series Triple Quadrupole MS with Version B.08.02 is used for calibration, compound
1029 optimization and sample data acquisition.

1030 A Waters Acquity UPLC BEH TSS C18 column (2.1 x 100mm, 1.7µm) column was used
1031 with mobile phase A) consisting of 0.1% formic acid in water; mobile phase (B) consisting of

1032 0.1% formic acid in acetonitrile. Gradient program: mobile phase (B) was held at 15% for 1
1033 min, increased to 55% in 19 min, then to 99% in 20 min and held for 2 min before going to
1034 initial condition and held for 4 min. The column was at 40℃ and 2 µl of sample was injected
1035 into the LC-MS with a flow rate of 0.3 ml/min. Calibration of the 6470 MS was achieved
1036 through Agilent ESI-Low Concentration Tuning Mix. Source parameters: Gas temp 300℃, Gas
1037 flow 5 l/min, Nebulizer 45 psi, Sheath gas temp 250℃, Sheath gas flow 11 l/min, Capillary -
1038 3500 V, Delta EMV -200 V. Dynamic MRM scan type is used with 0.07 min peak width.
1039 dMRM transitions and other parameters for each compound were list in a separate sheet. Delta
1040 retention time of plus and minus 1 min, fragmentor of 40 eV and cell accelerator of 5 eV were
1041 incorporated in the method. Data analysis was performed by Agilent Mass Hunter Quantitative
1042 Analysis for QQQ B.10.00 for integration. Results were exported to CVS file for further
1043 analysis.

1044 **Lamina propria cell extraction and flow cytometry analysis**

1045 Cecal and colonic lamina propria cells were extracted using the Lamina Propria
1046 Dissociation Kit and gentleMACS Dissociators (Miltenyi Biotec, Germany) according to the
1047 manufacturer's instruction. After digestion, cells were resuspended in PB buffer (PBS, pH 7.2,
1048 0.5 % BSA) and counted. For analysis of T cells and NK cells with the expression of
1049 transcription factors, the FOXP3/Transcription Factor Staining Buffer kit (eBioscences – 00-
1050 5523-00) was used along with the following anti-mouse antibodies: BV605-conjugated anti-CD4
1051 (Biolegend, RM4-5; 1/700), BV650-conjugated anti-B220 (BD Biosciences, RA3-6B2; 1/88),
1052 BV711-conjugated anti-CD3 (Biolegend, 17A2; 1/88), BV780-conjugated anti-CD45 (BD
1053 Biosciences, 30-F11; 1/88), FITC-conjugated anti-CD335/NKp46 (Biolegend, 29A1.4; 1/100),
1054 PE-Cy5-conjugated anti-CD8 (Biolegend, 53-6.7; 1/700), eF450-conjugated anti-FoxP3
1055 (eBiosciences, FJK-16s; 1/200), PE-conjugated anti-GATA3 (Biolegend, 16E10A23; 1/44), PE-
1056 eF610-conjugated anti-EOMES (eBiosciences, Dan11mag; 1/100), PE-Cy7 -conjugated anti-
1057 Tbet (Biolegend, 4B10; 1/44), APC-conjugated anti-RORgt (eBiosciences, AFKJS-9; 1/22). For
1058 B cells analysis and immunoglobulin expression, the BD Cytofix/Cytoperm™
1059 Fixation/Permeabilization Solution Kit (BD Biosciences – 554714) was used along with the
1060 following anti-mouse antibodies: eF450-conjugated anti-B220/CD45R (eBiosciences, RA3-6B2;
1061 1/700), eF506-conjugated anti-CD19 (eBiosciences, 1D3; 1/88), BV711-conjugated anti-CD3
1062 (Biolegend, 17A2; 1/88), BV780-conjugated anti-CD45 (BD Biosciences, 30-F11; 1/88), APC-

1063 conjugated anti-CD138 (Biolegend, 281-2; 1/100), FITC-conjugated anti-IgA (eBiosciences,
1064 mA-6E1; 1/700), PerCP-Cy5.5-conjugated anti-IgD (Biolegend, 11-26c.2a; 1/200), PE-
1065 conjugated anti-IgE (Biolegend, RME-1; 1/44), PE-Cy5-conjugated anti-IgM (BD Biosciences,
1066 R6-60.2; 1/100), PE-Cy7 -conjugated anti-IgG (Biolegend, Poly4053; 1/44). Breifly, 1.5 million
1067 cells were washed twice with PBS prior to 15 min of staining with the Zombie NIR™ Fixable
1068 Viability dye (BioLegend – 423105), followed by 2 washes with FACS Buffer (PBS, 5% fetal
1069 bovine serum) and fixation according to manufacturer instructions. Cells were then incubated at
1070 4°C for 15 min with Fc Block (Rat anti-mouse CD16 and CD32; BD Pharmingen – Cat.553141)
1071 and 30 min with the antibody mixes. Both Fc Block and antibodies were diluted in the
1072 permeabilization buffer provided with the fixation kits. Finally, cells were washed twice in their
1073 respective permeabilization buffer and resuspended in FACS Buffer for acquisition on a
1074 NovoCyte Quanteon Flow Cytometer System (Agilent). The data were then analyzed on FlowJo.

1075 **Analysis of IgA-coating of bacteria and sorting**

1076 Frozen fecal samples were homogeneized in 1 ml ice-cold PBS and centrifuged for 3 min
1077 at 100g, 4°C. Supernatant was filtered through a 70 µm straining sieve and centrifuged for 5 min
1078 at 10,000g, 4 °C. The pellet was resupended in 1 ml ice-cold PBS, the OD_{600} detected on a
1079 Nanodrop and the amount of bacteria computed as follow: 2 OD_{600} = 10^9 bacteria. Bacteria were
1080 pelleted again for 5 min at 10,000g, 4 °C, and resuspended in 500 µl of staining buffer (PBS, 5%
1081 goat serum). After 20 min of incubation on ice, $1x10^9$ bacteria were washed with 1 ml ice-cold
1082 PBS and stained for 30 min at 4°C with 4 µg of FITC-conjugated anti-mouse IgA antibody
1083 (Southern Biotech) in 100 µl of staining buffer. Cells were then washed once and resupended in
1084 1 ml PBS, and 100 µl of bacteria was pelleted and frozen until further analysis. Remaining
1085 bacteria where centrifuged and resuspended in 90 µl of staining buffer and 10 µL of anti-FITC
1086 MicroBeads. After 15 minutes of incubation at 4°C, bacteria were washed, resuspended in 500 µl
1087 of staining buffer and applied onto a LS column for sorting of IgA^+ and IgA^- fractions with a
1088 QuadroMACS™ Separator (Miltenyi Biotec). IgA-coated and IgA-uncoated fractions were
1089 centrifuged and dry pellets were stored at -80°C until further analysis. For analysis of IgA
1090 coating of bacteria, frozen pellets were defrost on ice and washed with 1 ml of staining buffer.
1091 Since all samples were not sorted at the same time, bacteria were stained again for 30 min with
1092 0.5 µg of FITC-conjugated anti-mouse IgA antibody (Southern Biotech) in 100 µl of staining
1093 buffer to refresh and harmonize the staining between batches. After a washing step, DNA was

1094 stained for 20 minutes with diluted 1:4000 in 200 µl of DNA staining solution (0.1 M HEPES,
1095 0.9 % NaCl, pH 7.2). Finally, bacteria were washed twice with PBS, fixed for 20 min in 4%
1096 PFA, washed again and analyzed on a NovoCyte Quanteon Flow Cytometer System (Agilent).
1097 Data were then analyzed on FlowJo. For analysis of IgA affinity, bacteria were treated with 200
1098 µl of PBS containing 3M NaSCN for 15 min at 4°C, 800rpm, prior to blocking and staining with
1099 FITC-conjugated anti-mouse IgA antibody as mentioned above.

1100 **Mucus measurements**

1101 The colons were sectioned from the colon-cecum junction to the anus, and immediately
1102 fixed in freshly made Carnoy's fixative (methanol:chloroform:glacial acetic acid, 60:30:10 v/v).
1103 The distal part of the small intestine was fixed in freshly made Carnoy's fixative together with
1104 the half blunt end of the cecum. Fixed tissues were kept in Carnoy's fixative for three hours and
1105 exchanged for fresh fixative for another 24 hours. The tissues were then washed in 100%
1106 methanol and kept until placed in cassettes for histology preparation. The remaining empty half
1107 of the cecum were flash frozen in liquid nitrogen and kept at -80°C until further use.

1108 Slides were deparaffinized by submerging in xylene (Sigma-Aldrich, USA) for five
1109 minutes, followed by another xylene incubation for five minutes. Afterward, the slides were
1110 dehydrated twice in 100% ethanol for 5 minutes. The slides were then quickly washed in Milli-Q
1111 water and antigens were retrieved by submerging in antigen retrieving solution (10 mM sodium
1112 citrate, pH 6.0). The submerged sections were heated to 90°C for 10 minutes and cooldown in
1113 room temperature for 20 minutes. Slides were quickly dipped three times in Milli-Q water and
1114 blotted to remove excess liquid. To better hold liquid, a PAP pen was used to draw around the
1115 tissue area for the subsequent steps. The sections were blocked by covering the tissue in blocking
1116 buffer (1:10 goat serum (Sigma, USA) in Tris-buffered Saline (TBS; 500 mM NaCl, 50 mM
1117 Tris, pH 7.4)) and incubated for an hour at room temperature. For the primary antibody staining,
1118 the tissue was covered with a 1:200 dilution of Mucin 2 antibody (H-300) (Santa Cruz
1119 Biotechnology, USA) in blocking buffer and incubated for two hours at room temperature.
1120 Following the incubation, the slides were rinsed three times in TBS, for five minutes each. The
1121 secondary antibody staining was performed by covering the tissue with a 1:200 dilution of Alexa
1122 Fluor 488 conjugated goat anti-rabbit IgG antibody (Thermo Fisher Scientific, USA) in blocking
1123 buffer for one hour at room temperature in dark. The tissue sections were washed twice in TBS
1124 for 5 minutes, gently blotted, and covered with ProLong Gold Antifade reagent with DAPI

1125 (Invitrogen, USA), covered with cover slips and sealed with nail polish. The slides were kept at
1126 room temperature for 24 hours in dark, then kept in 4°C until imaging. The mucus layer in the
1127 sections were visualized using a Zeiss Apotome by taking pictures across fecal pellets and
1128 stitching the images together to compose a single image. Mucus layer measurements were
1129 performed by using BacSpace as described by Earle et al.

1130 **Histological examination of intestinal tissue sections**

1131 Extent of histologic lesions was scored on a semi-quantitative basis by a trained
1132 pathologist (KE) in a blinded fashion, using a modification of the scoring system of Bugni *et al*.
1133 [45]. Inflammation, epithelial damage, epithelial hyperplasia and dysplasia and the presence or
1134 absence of submucosa edema were scored on a scale of 1-4 according to the following table.
1135 Scores for each category were added to determine a total score. Cecum and colon were scored
1136 separately.

Score	**0**	**1**	**2**	**3**	**4**
inflammation	Normal	Scattered PMNs or plasma cells in lamina propria or submucosa	Coalescing mucosal and/or submucosal inflammation	Widespread submucosal inflammation	Severe diffuse transmural inflammation
epithelial damage	None	Focally dilated glands and/or attenuated surface epithelium, and/or clusters of sloughed cells in lumen	Focally extensive gland dilation and/or surface epithelial attenuation, many sloughed cells in lumen	Mucosa erosions	Mucosal ulceration
hyperplasia/ dysplasia	Normal	Hypertrophy and/or hyperplasia present	Cellular and/or glandular dysplasia present		
Submucosal edema	Absent	Present			

1137

1138 **Mucus penetrability assay**

1139 Penetrability of the colonic mucus was assessed as described by Gustafsson et al [21].
1140 Briefly, colons were flushed with ice-cold oxygenated KREBS Buffer (116 mM NaCl, 1.3 mM
1141 $CaCl_2$, 3.6 mM KCl, 1.4 mM KH_2PO_4, 23 mM $NaHCO_3$, and 1.2 $MgSO_4$ – Carl Roth) and
1142 opened along the mesenteric axis. The longitudinal muscle layer was removed by blunt

1143 dissection and the distal mucosa was inserted in a perfusion chamber. The basolateral chamber
1144 was filled with 0.6 µg/ml SYTO9 (Fisher Scientific - 10237582) in oxygenated KREBS Glucose
1145 Buffer (KREBS Buffer containing 10mM Glucose, 5.7 mM sodium pyruvate and 5.1 mM
1146 sodium-l-glutamate), and the apical chamber was filled with oxygenated KREBS Mannitol
1147 Buffer (KREBS Buffer, containing 10mM Mannitol, 5.7 mM sodium pyruvate and 5.1 mM
1148 sodium-l-glutamate). After 10 min incubation in the dark at room temperature, FluoSphere™
1149 carboxylate beads (1µm, red 580/605 – Invitrogen – F882) were applied on top and let to
1150 sediment on the tissue for 5 min in the dark at room temperature. The apical chamber was then
1151 gently washed several times to remove excess of beads. The chamber was incubated for 10 min
1152 in the dark before being visualized with a microscope. For each tissue, 4-7 confocal images were
1153 taken in XY stacks from the epithelium at the bottom to the beads on top, with 5 µm-intervals
1154 between sections. Images were then analyzed with Imaris software, and the penetrability was
1155 computed by comparing the distance between the outer border of the beads and the epithelium
1156 with the distance between the most inner beads and the epithelium.

1157 **16S rRNA gene-based community analysis**

1158 PCR and library preparation were performed by the University of Michigan Microbiome
1159 Core lab as described by Kozich et al. [46]. The V4 region of the 16S rRNA gene was amplified
1160 using the dual-index primers described by Kozich et al, 2013. The normalized and amplicon size
1161 evaluated samples were sequenced using an Illumina MiSeq. The raw sequences were analyzed
1162 using mothur v1.42.3 [47] with the included controls: PBS control during the sequencing and
1163 ZymoBIOMICS Microbial Community DNA Standard (cat# D6306) for error analysis.
1164 Sequences were aligned to the reference Silva database version 132 for contamination analysis
1165 and SPF experiments. Moreover, gnotobiotic mice sequences were also aligned to a custom
1166 reference database containing the 16S v4 region from each of the 14 bacteria members. The R
1167 package "vegan" was used to calculate the principal component analysis from the Bray-Curtis
1168 dissimilarity index.
1169
1170

Figure 1

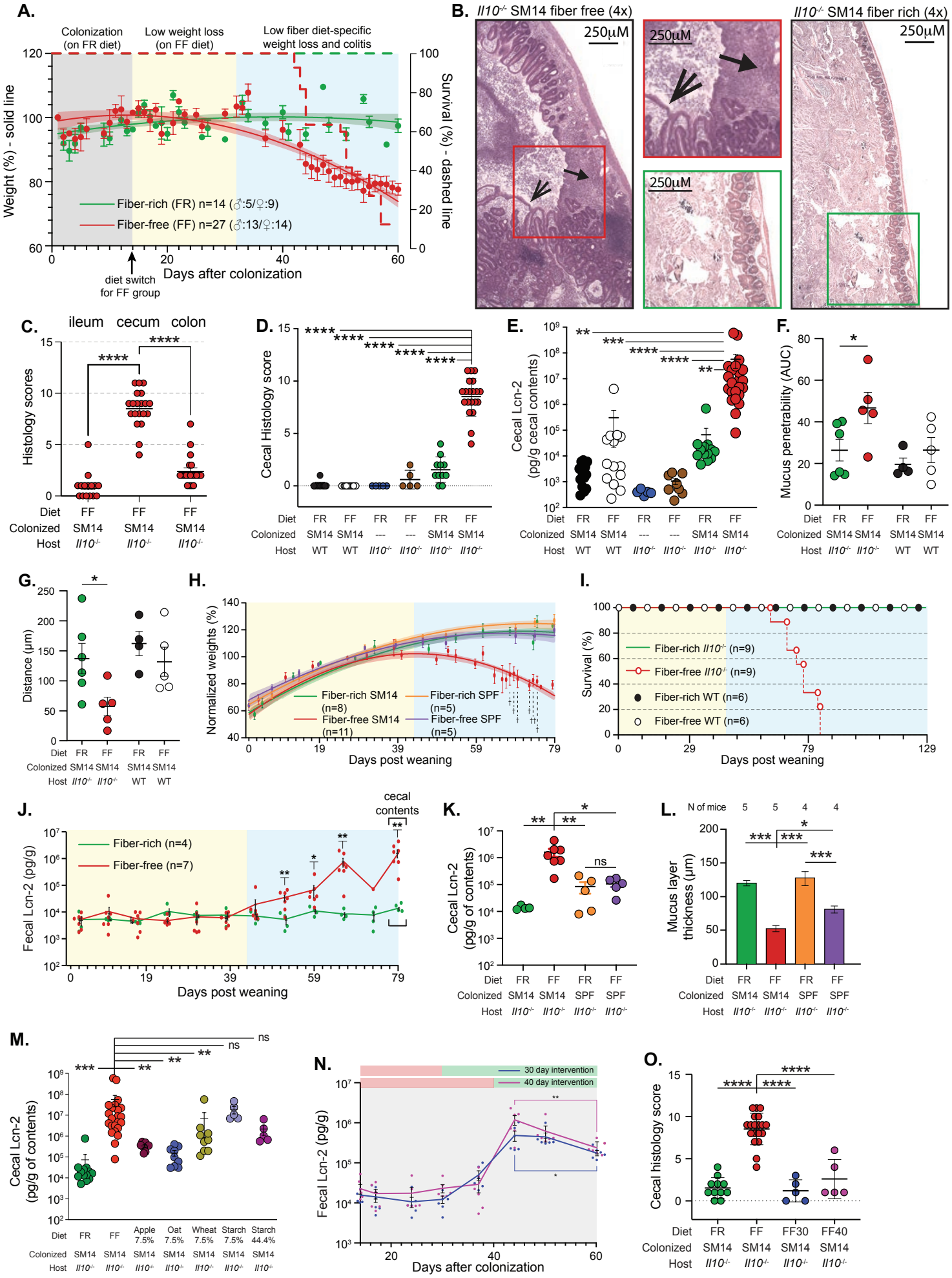
A.
Colonization (on FR diet)
Low weight loss (on FF diet)
Low fiber diet-specific weight loss and colitis
Weight (%) - solid line
Survival (%) - dashed line
Fiber-rich (FR) n=14 (♂:5/♀:9)
Fiber-free (FF) n=27 (♂:13/♀:14)
diet switch for FF group
Days after colonization
B.
Il10-/- SM14 fiber free (4x)
Il10-/- SM14 fiber rich (4x)
250µM
C.
ileum cecum colon
Histology scores
D.
Cecal Histology score
E.
Cecal Lcn-2 (pg/g cecal contents)
F.
Mucus penetrability (AUC)
G.
Distance (µm)
H.
Normalized weights (%)
Fiber-rich SM14 (n=8)
Fiber-free SM14 (n=11)
Fiber-rich SPF (n=5)
Fiber-free SPF (n=5)
Days post weaning
I.
Survival (%)
Fiber-rich Il10-/- (n=9)
Fiber-free Il10-/- (n=9)
Fiber-rich WT (n=6)
Fiber-free WT (n=6)
Days post weaning
J.
cecal contents
Fecal Lcn-2 (pg/g)
Fiber-rich (n=4)
Fiber-free (n=7)
Days post weaning
K.
Cecal Lcn-2 (pg/g of contents)
L.
N of mice
Mucus layer thickness (µm)
M.
Cecal Lcn-2 (pg/g of contents)
N.
30 day intervention
40 day intervention
Fecal Lcn-2 (pg/g)
Days after colonization
O.
Cecal histology score
Diet
Colonized
Host

Figure 2

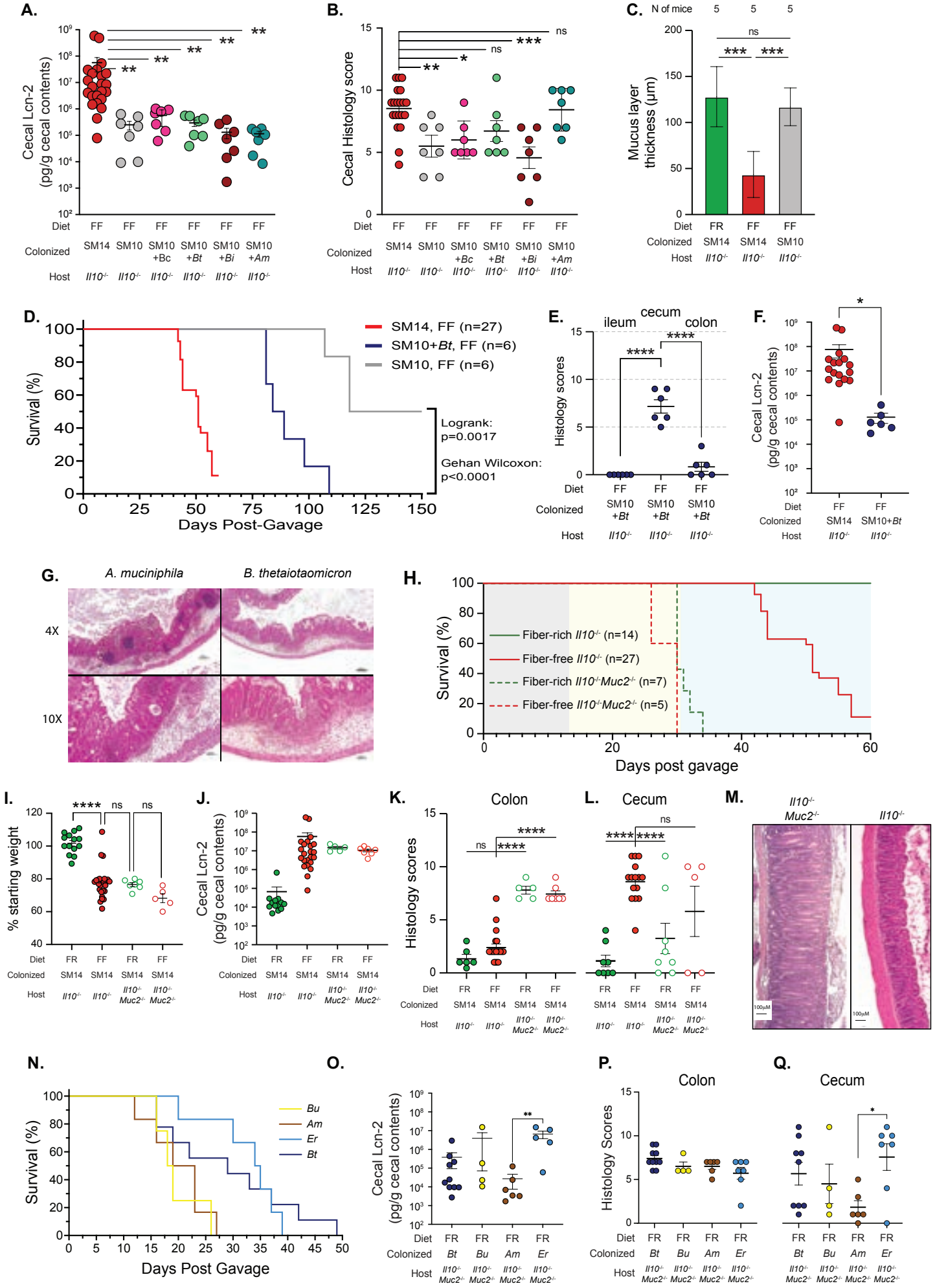
A.
Cecal Lcn-2 (pg/g cecal contents)
Diet FF FF FF FF FF FF
Colonized SM14 SM10 SM10 +Bc SM10 +Bt SM10 +Bi SM10 +Am
Host Il10-/- Il10-/- Il10-/- Il10-/- Il10-/- Il10-/-
B.
Cecal Histology score
C.
N of mice 5 5 5
Mucus layer thickness (µm)
Diet FR FF FF
Colonized SM14 SM14 SM10
Host Il10-/- Il10-/- Il10-/-
D.
Survival (%)
Days Post-Gavage
SM14, FF (n=27)
SM10+Bt, FF (n=6)
SM10, FF (n=6)
Logrank: p=0.0017
Gehan Wilcoxon: p<0.0001
E.
ileum cecum colon
Histology scores
Diet FF FF FF
Colonized SM10 +Bt SM10 +Bt SM10 +Bt
Host Il10-/- Il10-/- Il10-/-
F.
Cecal Lcn-2 (pg/g cecal contents)
Diet FF FF
Colonized SM14 SM10+Bt
Host Il10-/- Il10-/-
G.
A. muciniphila
B. thetaiotaomicron
4X
10X
H.
Survival (%)
Days post gavage
Fiber-rich Il10-/- (n=14)
Fiber-free Il10-/- (n=27)
Fiber-rich Il10-/-Muc2-/- (n=7)
Fiber-free Il10-/-Muc2-/- (n=5)
I.
% starting weight
Diet FR FF FR FF
Colonized SM14 SM14 SM14 SM14
Host Il10-/- Il10-/- Il10-/- Muc2-/- Il10-/- Muc2-/-
J.
Cecal Lcn-2 (pg/g cecal contents)
K.
Colon
Histology scores
L.
Cecum
M.
Il10-/- Muc2-/-
Il10-/-
N.
Survival (%)
Days Post Gavage
Bu
Am
Er
Bt
O.
Cecal Lcn-2 (pg/g cecal contents)
Diet FR FR FR FR
Colonized Bt Bu Am Er
Host Il10-/- Muc2-/- Il10-/- Muc2-/- Il10-/- Muc2-/- Il10-/- Muc2-/-
P.
Colon
Histology Scores
Q.
Cecum

Figure 3

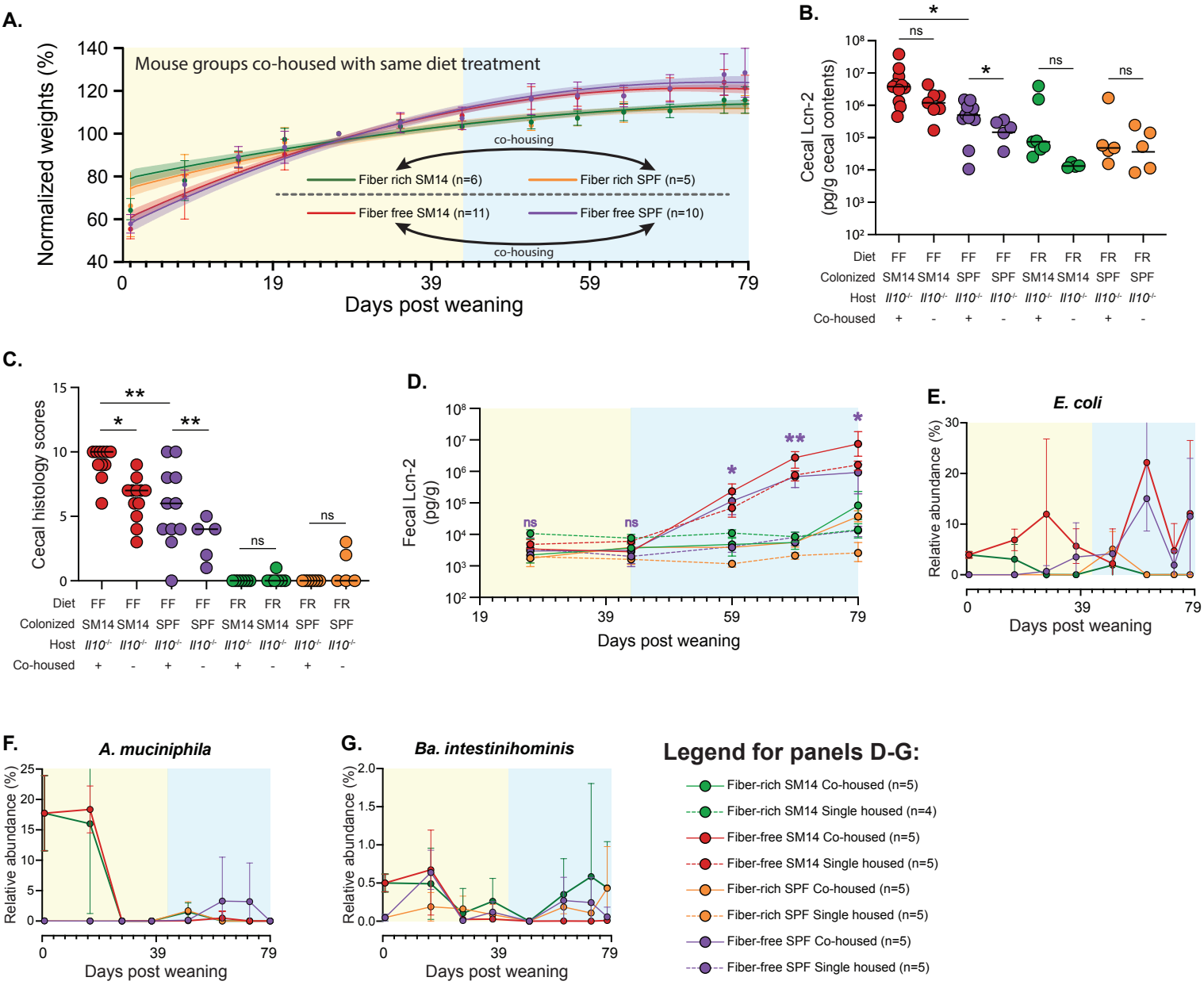
A.
Mouse groups co-housed with same diet treatment
Normalized weights (%)
Days post weaning
co-housing
Fiber rich SM14 (n=6)
Fiber rich SPF (n=5)
Fiber free SM14 (n=11)
Fiber free SPF (n=10)
B.
Cecal Lcn-2 (pg/g cecal contents)
Diet FF FF FF FF FR FR FR FR
Colonized SM14 SM14 SPF SPF SM14 SM14 SPF SPF
Host Il10-/- Il10-/- Il10-/- Il10-/- Il10-/- Il10-/- Il10-/- Il10-/-
Co-housed + - + - + - + -
C.
Cecal histology scores
D.
Fecal Lcn-2 (pg/g)
Days post weaning
E.
E. coli
Relative abundance (%)
Days post weaning

F.
A. muciniphila
Relative abundance (%)
Days post weaning
G.
Ba. intestinihominis
Relative abundance (%)
Days post weaning
Legend for panels D-G:
Fiber-rich SM14 Co-housed (n=5)
Fiber-rich SM14 Single housed (n=4)
Fiber-free SM14 Co-housed (n=5)
Fiber-free SM14 Single housed (n=5)
Fiber-rich SPF Co-housed (n=5)
Fiber-rich SPF Single housed (n=5)
Fiber-free SPF Co-housed (n=5)
Fiber-free SPF Single housed (n=5)

Figure 4

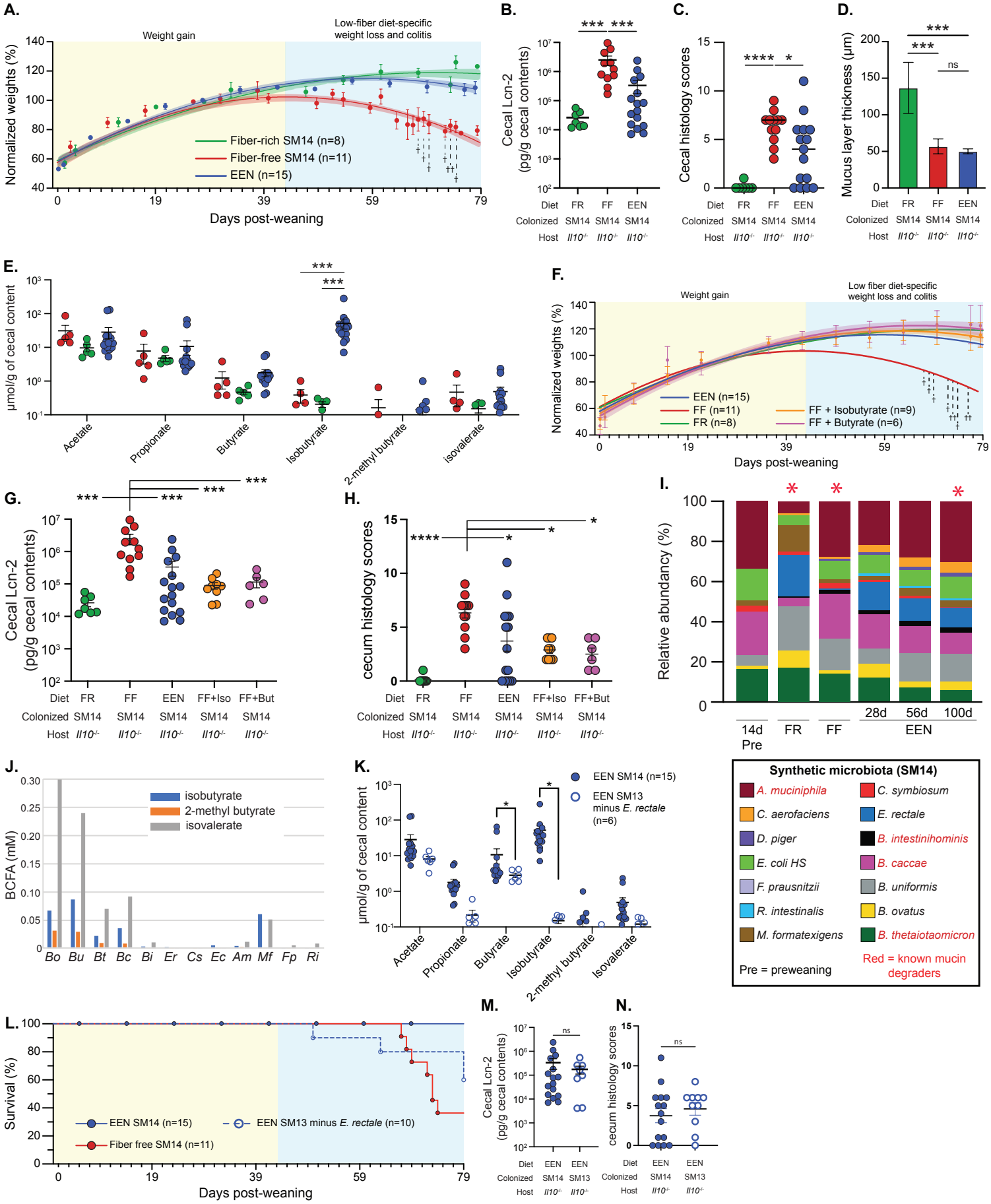
A.
Weight gain
Low-fiber diet-specific weight loss and colitis
Normalized weights (%)
Days post-weaning
Fiber-rich SM14 (n=8)
Fiber-free SM14 (n=11)
EEN (n=15)
B.
Cecal Lcn-2 (pg/g cecal contents)
C.
Cecal histology scores
D.
Mucus layer thickness (µm)
ns
Diet FR FF EEN
Colonized SM14 SM14 SM14
Host Il10-/- Il10-/- Il10-/-
E.
µmol/g of cecal content
Acetate
Propionate
Butyrate
Isobutyrate
2-methyl butyrate
isovalerate
F.
EEN (n=15)
FF (n=11)
FR (n=8)
FF + Isobutyrate (n=9)
FF + Butyrate (n=6)
G.
Cecal Lcn-2 (pg/g cecal contents)
Diet FR FF EEN FF+Iso FF+But
Colonized SM14 SM14 SM14 SM14 SM14
Host Il10-/- Il10-/- Il10-/- Il10-/- Il10-/-
H.
cecum histology scores
I.
Relative abundancy (%)
14d Pre
FR
FF
28d
56d
100d
EEN
J.
BCFA (mM)
isobutyrate
2-methyl butyrate
isovalerate
Bo Bu Bt Bc Bi Er Cs Ec Am Mf Fp Ri
K.
µmol/g of cecal content
EEN SM14 (n=15)
EEN SM13 minus E. rectale (n=6)
Acetate
Propionate
Butyrate
Isobutyrate
2-methyl butyrate
Isovalerate
Synthetic microbiota (SM14)
A. muciniphila
C. symbiosum
C. aerofaciens
E. rectale
D. piger
B. intestinihominis
E. coli HS
B. caccae
F. prausnitzii
B. uniformis
R. intestinalis
B. ovatus
M. formatexigens
B. thetaiotaomicron
Pre = preweaning
Red = known mucin degraders
L.
Survival (%)
EEN SM14 (n=15)
EEN SM13 minus E. rectale (n=10)
Fiber free SM14 (n=11)
Days post-weaning
M.
Cecal Lcn-2 (pg/g cecal contents)
Diet EEN EEN
Colonized SM14 SM13
Host Il10-/- Il10-/-
N.
cecum histology scores
Diet EEN EEN
Colonized SM14 SM13
Host Il10-/- Il10-/-

Figure 5

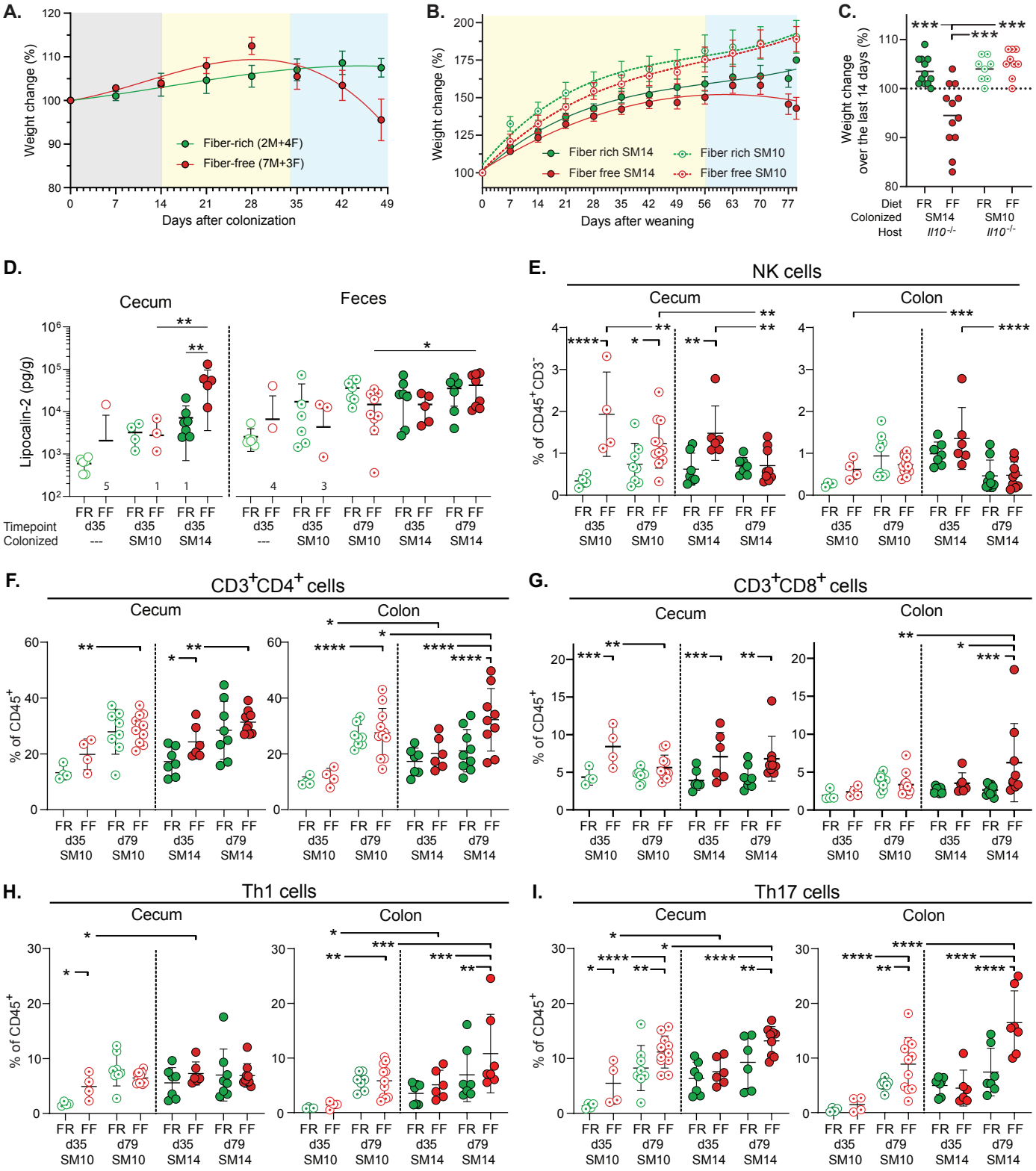
A.
Weight change (%)
Days after colonization
Fiber-rich (2M+4F)
Fiber-free (7M+3F)
B.
Weight change (%)
Days after weaning
Fiber rich SM14
Fiber free SM14
Fiber rich SM10
Fiber free SM10
C.
Weight change over the last 14 days (%)
Diet
Colonized
Host
D.
Cecum
Feces
Lipocalin-2 (pg/g)
Timepoint
Colonized
E.
NK cells
Cecum
Colon
% of CD45+CD3-
F.
CD3+CD4+ cells
Cecum
Colon
% of CD45+
G.
CD3+CD8+ cells
Cecum
Colon
% of CD45+
H.
Th1 cells
Cecum
Colon
% of CD45+
I.
Th17 cells
Cecum
Colon
% of CD45+

Figure 6

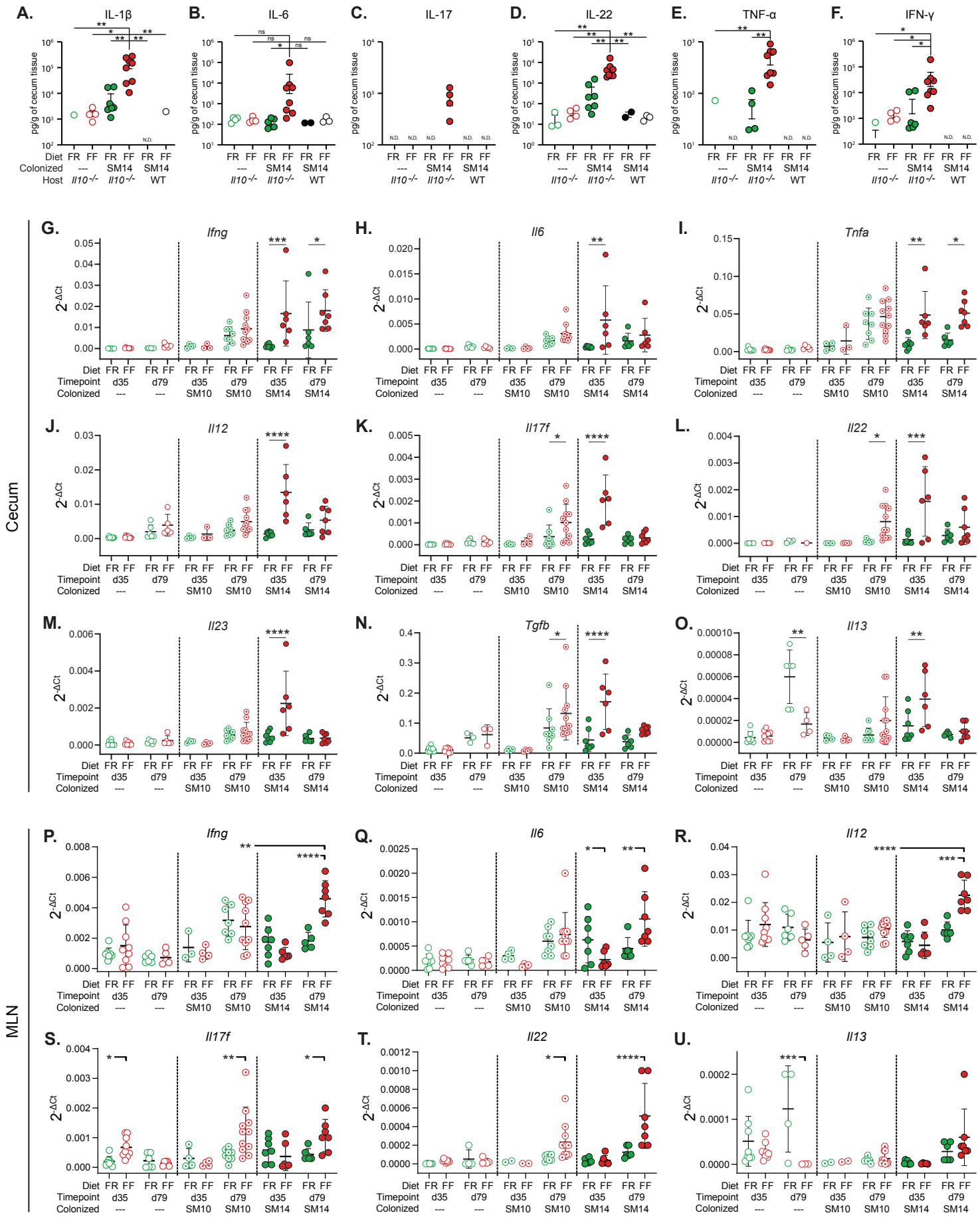
A. IL-1β
B. IL-6
C. IL-17
D. IL-22
E. TNF-α
F. IFN-γ
pg/g of cecum tissue
Diet FR FF FR FF FR FF
Colonized --- SM14 SM14
Host Il10-/- Il10-/- WT
N.D.
Cecum
G. Ifng
H. Il6
I. Tnfa
J. Il12
K. Il17f
L. Il22
M. Il23
N. Tgfb
O. Il13
2-ΔCt
Diet FR FF FR FF FR FF FR FF FR FF
Timepoint d35 d79 d35 d79 d35 d79
Colonized --- --- SM10 SM10 SM14 SM14
MLN
P. Ifng
Q. Il6
R. Il12
S. Il17f
T. Il22
U. Il13

Figure 7

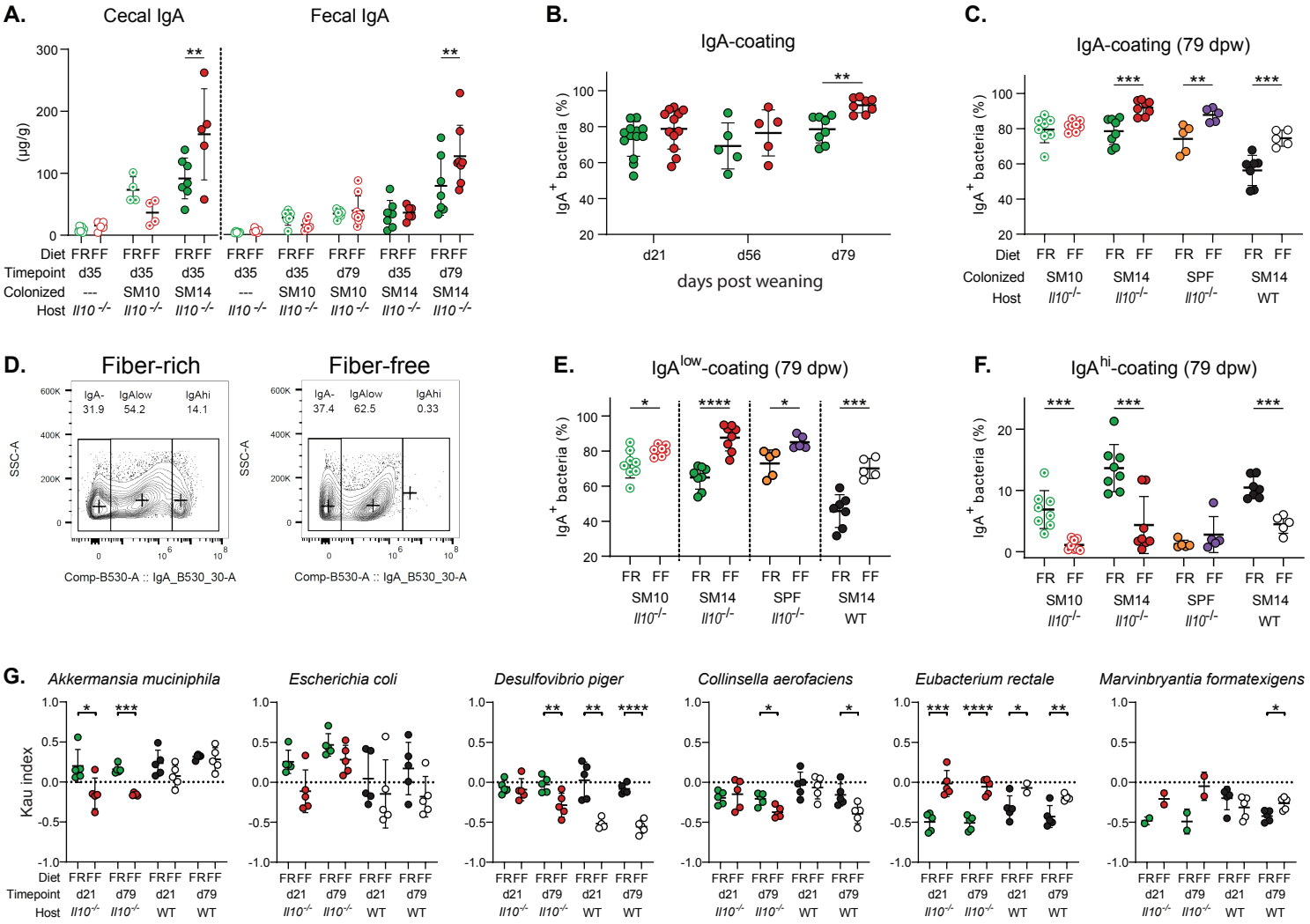
A.
Cecal IgA
Fecal IgA
(µg/g)
Diet FRFF FRFF FRFF FRFF FRFF FRFF FRFF FRFF
Timepoint d35 d35 d35 d35 d35 d79 d35 d79
Colonized --- SM10 SM14 --- SM10 SM10 SM14 SM14
Host Il10 -/- Il10 -/- Il10 -/- Il10 -/- Il10 -/- Il10 -/- Il10 -/- Il10 -/-
B.
IgA-coating
IgA+ bacteria (%)
days post weaning
d21
d56
d79
C.
IgA-coating (79 dpw)
Diet FR FF FR FF FR FF FR FF
Colonized SM10 SM14 SPF SM14
Host Il10-/- Il10-/- Il10-/- WT
D.
Fiber-rich
Fiber-free
IgA- IgAlow IgAhi
31.9 54.2 14.1
37.4 62.5 0.33
SSC-A
Comp-B530-A :: IgA_B530_30-A
E.
IgAlow-coating (79 dpw)
F.
IgAhi-coating (79 dpw)
G.
Akkermansia muciniphila
Escherichia coli
Desulfovibrio piger
Collinsella aerofaciens
Eubacterium rectale
Marvinbryantia formatexigens
Kau index
Diet FRFF FRFF FRFF FRFF
Timepoint d21 d79 d21 d79
Host Il10-/- Il10-/- WT WT

Supplemental Figure 1

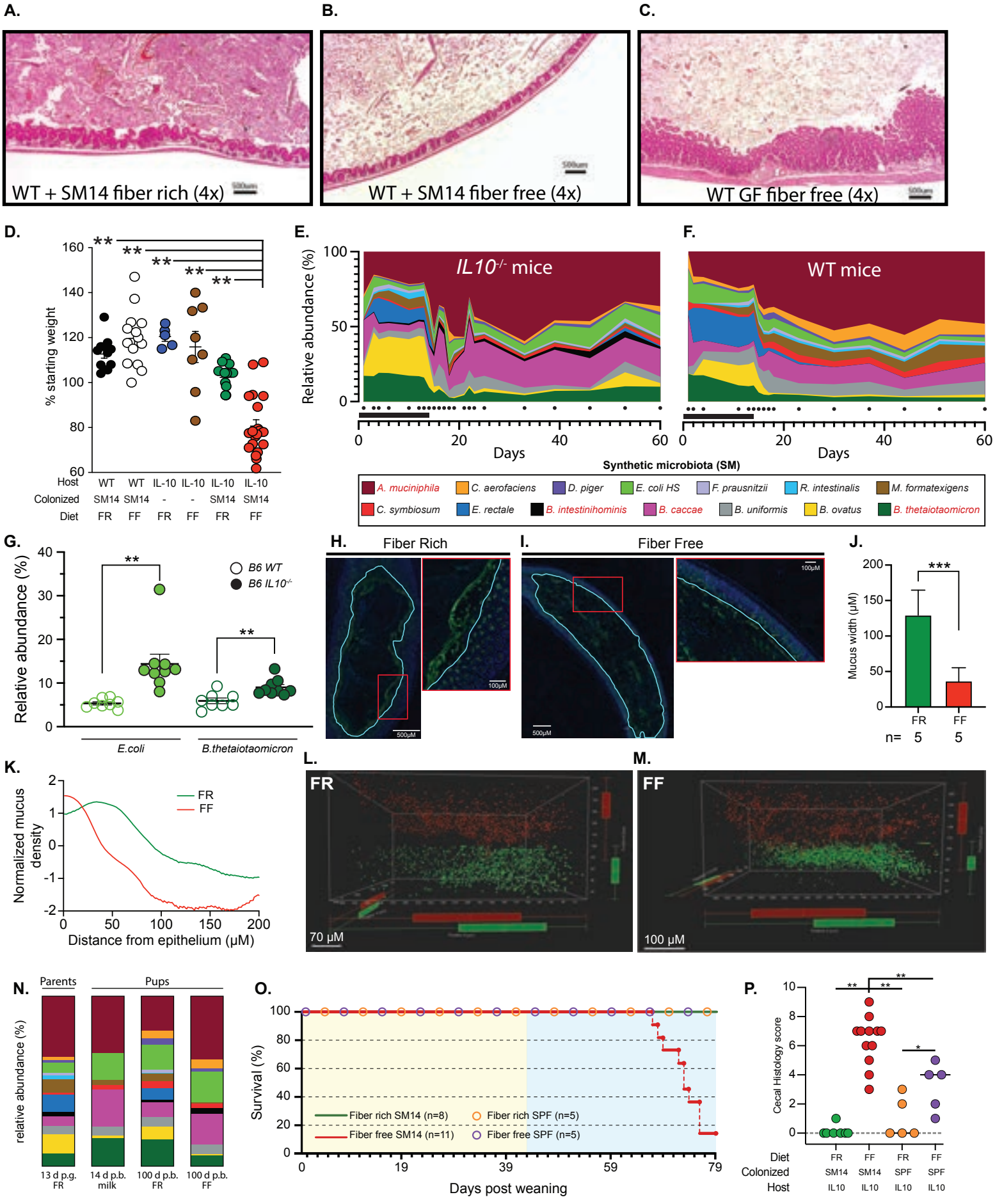

Supplemental Figure 2

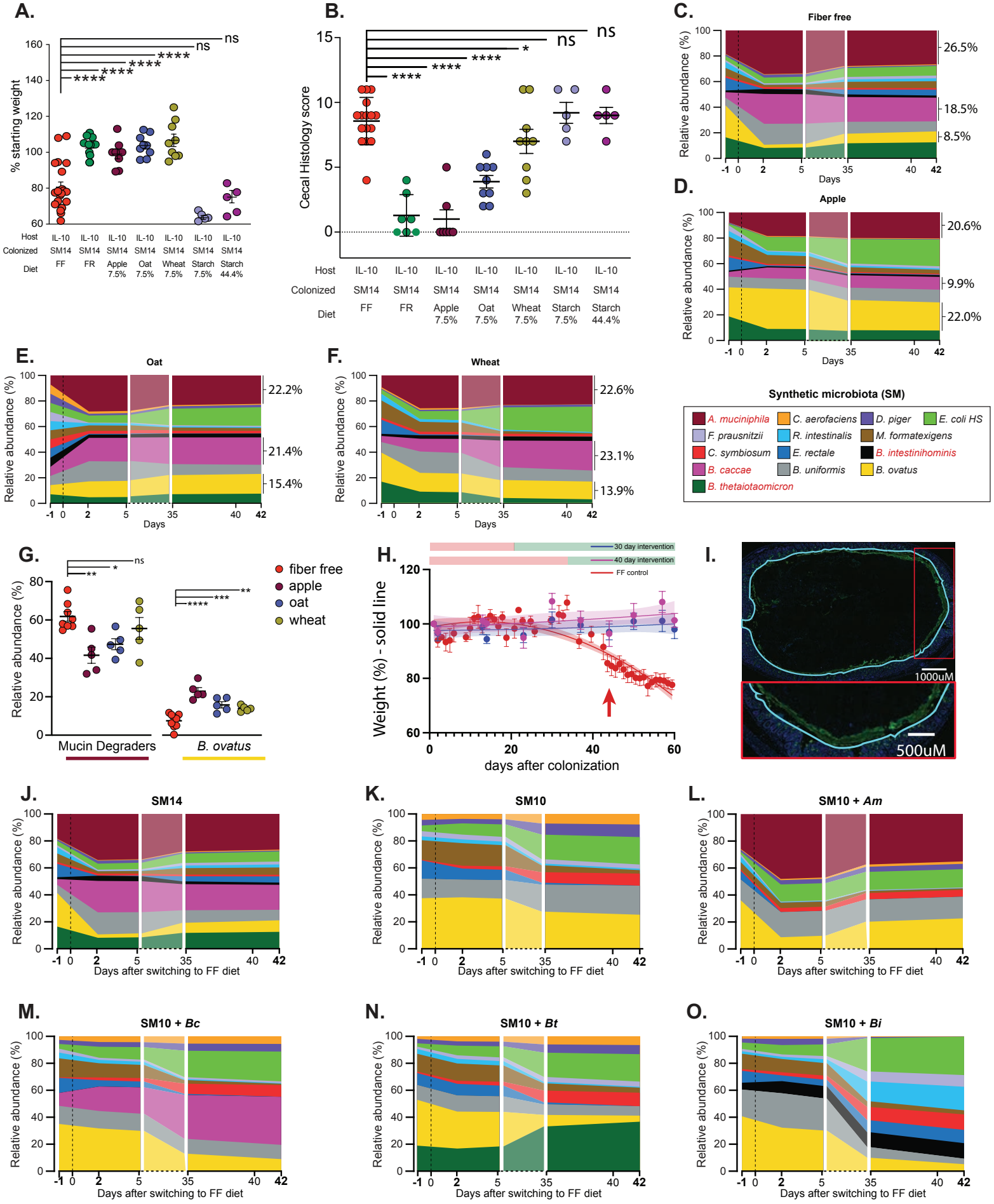

Supplemental Figure 3

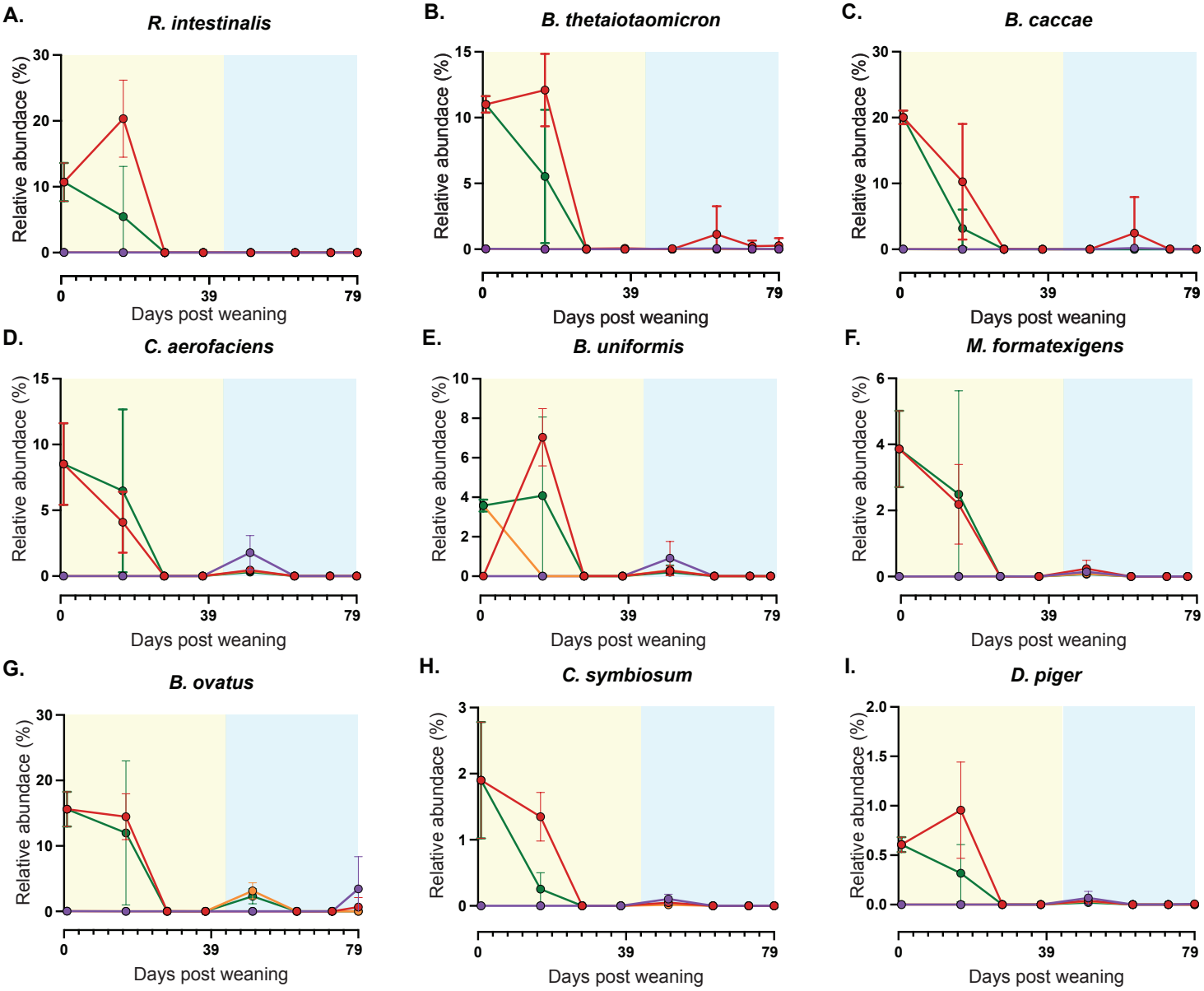

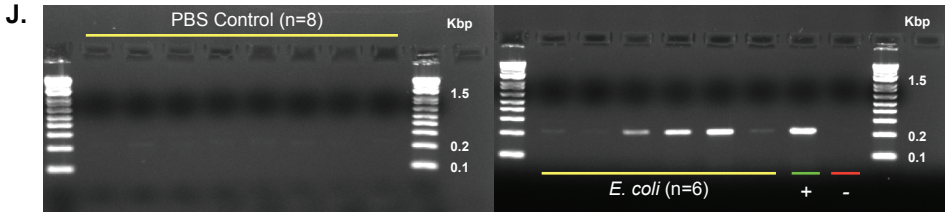

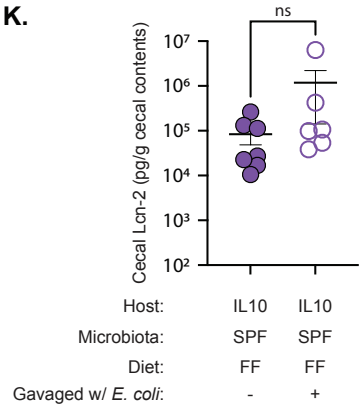

Supplemental Figure 4

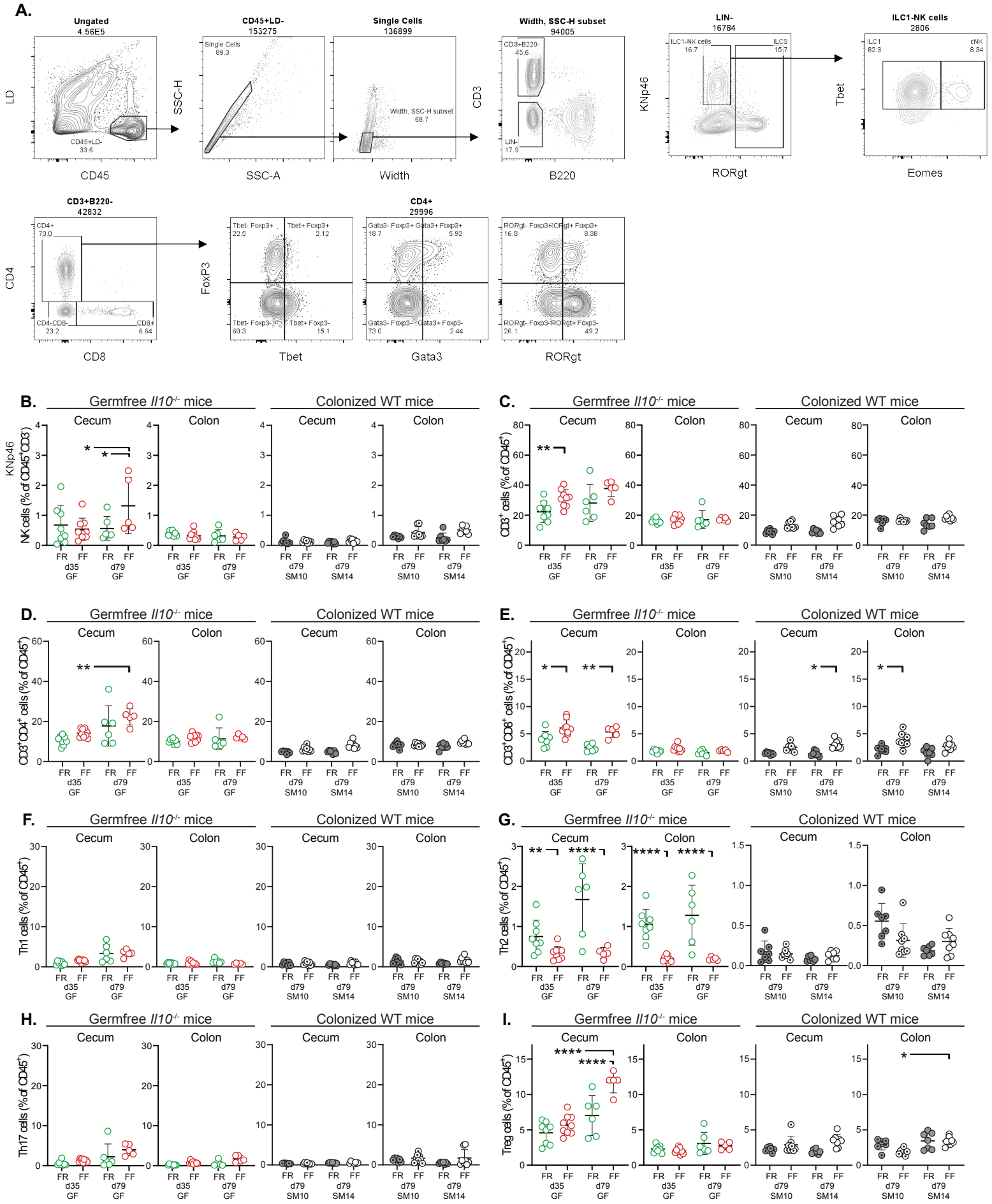

Supplemental Figure 5

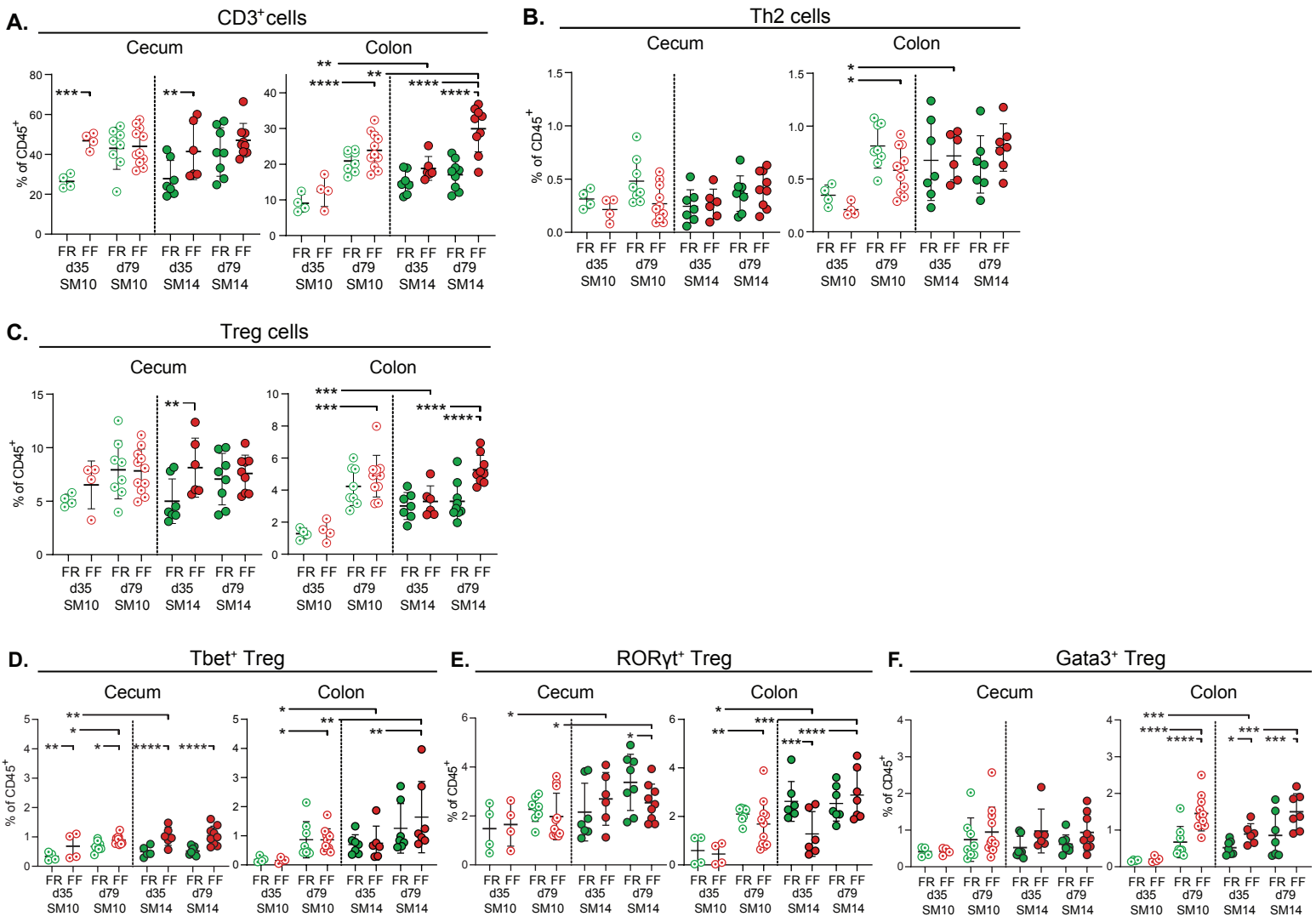

Supplemental Figure 6

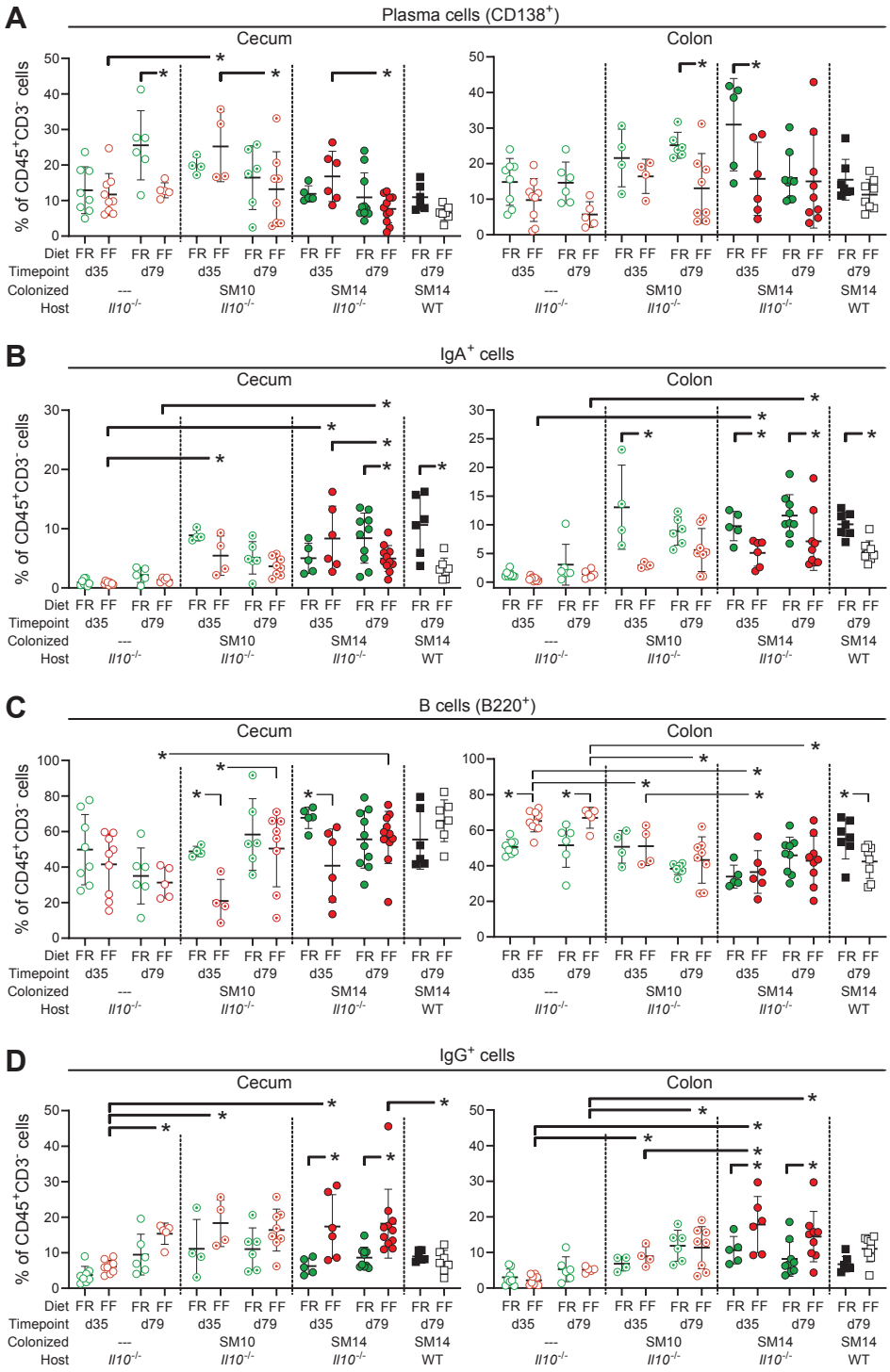
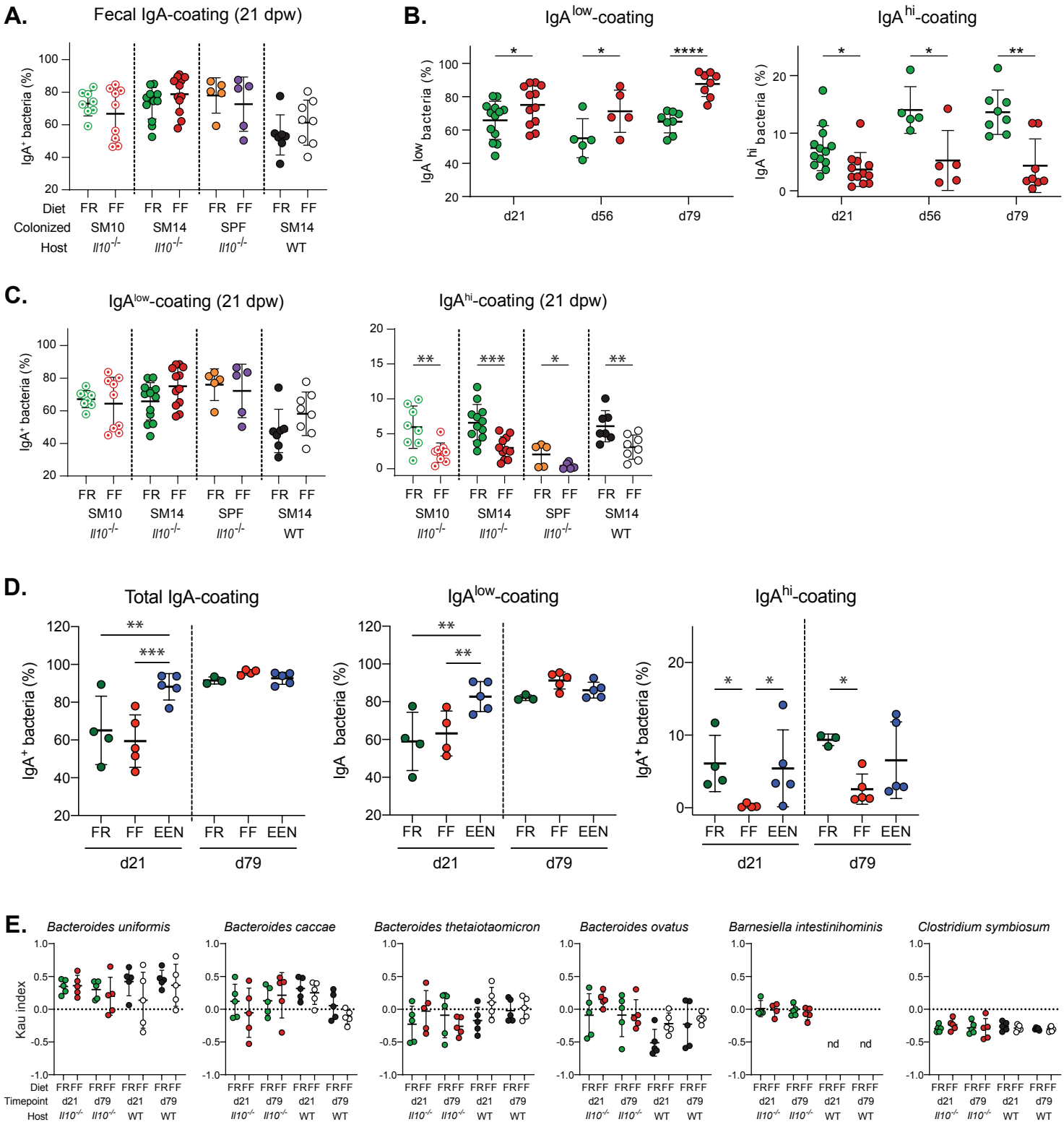
Supplemental Figure 7